Optimizing Antenna Gain

With a Metamaterial Filter

_____

A Thesis

presented to

the Faculty of the Graduate School

at the University of Missouri-Columbia

_____

In Partial Fulfillment

of the Requirements for the Degree

Master of Science

_____

by

JULIAN BAKER

Dr. Naz E. Islam, Thesis Supervisor

JULY 2011

The undersigned, appointed by the dean of the Graduate School, have examined the thesis entitled

Optimizing Antenna Gain With a Metamaterial Filter

presented by Julian Baker,

a candidate for the degree of Master of Science, and hereby certify that, in their opinion, it is worthy of acceptance.

_____

Professor Naz E. Islam

_____

Professor Robert O'Connell

_____

Professor Haskell Taub

…….……Thanks, dad for helping me out when I needed it, and fighting through all your health problems to see me get this far.

ACKNOWLEDGEMENTS

TABLE OF CONTENTS

LIST OF FIGURES

METAMATERIALS LENS GAIN ENHANCEMENT AND POWER APPLICATIONS

Julian Baker

Dr. Naz Islam, Dissertation Supervisor

ABSTRACT

Metamaterials are man-made structures, usually designed by placing electromagnetic resonators, such as split ring resonators (SRRs), in a periodic array. Metamaterials also exhibit lensing properties, and, when placed next to antennas, are known to improve the gain of the antenna. For high power antennas, the placement of metamaterials with embedded metallic resonators, however, may lead to excessive heating effects and alternative solutions need to be developed.

In this research work, a metamaterial lens constructed from cubic high dielectric resonators (CHDR) embedded in a low dielectric slab was placed in front of a circular patch and a fractal patch antenna respectively, in order to characterize the effects on the antenna parameters, specifically the gain, as a result of the antenna and lens coupling. The CHDR based metamaterial lens was designed to have a negative refractive index at 10.4 GHz, which was determined through the extraction of the constitutive parameters from the s-parameters. The optimum distance of lens placement was then determined in order to maximize the antenna gain for both cases. Heating effects at high power were also demonstrated through a comparison of the CHDR based metamaterial with a SRR based structure.

A methodology for optimizing the metamaterial lens design is also presented, which is based on the Drude dispersion model applied to a homogeneous metamaterial.

The model determines the optimum placement and geometry of the metamaterial lens in order to maximize antenna gain for a source radiating spherical electromagnetic waves. Finally, in order to demonstrate the advantages of a CHDR based metamaterial lens over a metallic split-ring resonator (SRR) based lens, for high power applications, the structures were subjected to electromagnetic radiation and their thermal properties were studied. All simulations were performed using CST microwave studio (a commercially available electromagnetic software suite).

The optimum placement of the metamaterial slab in front of the circular patch antenna and the fractal patch antenna for maximum gain enhancement was determined to be 14 mm, and 18 mm respectively. The gain improvement for the circular patch antenna was from 7.380 dB to 11.75 dB, and the gain improvement for the fractal patch antenna was from 8.980 dB to 12.28 dB.

In a separate but related study, a metamaterial lens was designed and analyzed through the Drude formulation and a concept to improve the directivity of an antenna through a special metamaterial lens design was presented. The main purpose of using the Drude model is to allow a user of CST Microwave Studio to indirectly set the values of the permittivity and permeability (i.e. the refractive index and absorption) at a given frequency, which are then used by the program to calculate the electromagnetic fields in time and space.

A homogenous metamaterial lens was analyzed through the Drude formulation, it was shown that if the source is radiating a spherical wave, the geometry of the metamaterial lens should be flat on the side in which the wave is entering and parabolic

on the side of the lens that the wave is exiting.   In addition, the optimum distance away

from the source was determined to be equal to the thickness of the rectangular portion of

the metamaterial lens.

Finally, in the lens heating study using SRR and CHDR resonators, it was found

that for a power factor of 65W and a background temperature of 300 K, an SRR based

lens has a maximum temperature of 1676.0 K, while the CHDR lens has a maximum

temperature of 300.16 K, demonstrating that the CHDR based lens is the preferred

metamaterial type for high power applications.   For compact high power applications

requiring high gain antennas without significant heating problems, a coupling of CHDR

based metamaterials and a fractal or patch antenna is a preferable and a viable candidate.

CHAPTER 1

INTRODUCTION

Often when a new concept is developed in physics, the results can be far reaching. The concept of metamaterials in based primarily on the concept of a material having a negative refractive index, which is something that was previously thought impossible. Such materials are not found in nature but can be manmade. This is achieved by placing resonators, like SRRs (split ring resonator), at regular intervals in a dielectric thus making the configuration dispersive. The embedded resonators and the dielectric have a negative refractive index at some given frequency, and are thus deemed metamaterials. On the surface, this realization of a negative refractive index may appear like a minor change; but some of the results from applying a negative refractive index are astonishing. One of the most incredible applications of metamaterials is their ability to make objects theoretically invisible to electromagnetic radiation at a given frequency. If this could be accomplished in practice, then a soldier could become invisible at optical frequencies. There are commercial applications to this cloaking ability of metamaterials in Electromagnetic compatibility EMC. In addition, a metamaterial can have a tunable refractive index. This means that the frequency at which the material acts like a metamaterial can change, and makes metamaterials application in areas such as biosensing possible (i.e. a dielectric in a metamaterial can be made from materials that can absorb fluids thereby changing the refractive index of the metamaterial). Indeed, the applications to both defense and commercial industries are immense; and, in the future, it

is likely that many more applications will be found. The details of the construction and analysis of such materials is discussed elsewhere in this work.

Following this brief introduction, the rest of this thesis is organized as follows. In this chapter, the basics of Electromagnetism, including Maxwell's equations, their solution method, metamaterial analysis and construction using various resonators, and the lensing effects of metamaterials are discussed. Chapter 2 deals with the construction and analysis of metamaterials, and also discusses the coupling of metamaterials with antennas and the gain enhancement. In chapter 3, the results of the analysis of antenna-metamaterial lens coupling are shown, and the heating effects analyzed for high power applications are also shown. Discussions of the results are presented in Chapter 4 while conclusions and recommendations for future research are presented in Chapter 5.

This research relates to the interaction of electromagnetic fields from an antenna with a metamaterial structure (lens); therefore a brief introduction to the basic tools used in the analysis is necessary. The following sections provide a background to Maxwell's equations, the wave equation, energy carried by the wave, bending and transmission of waves as it travels through different media, and antennas as the generator of electromagnetic waves. The concept of metamaterials, split ring and other resonators that are used in manmade metamaterials, and the metamaterial lens is also introduced in this chapter.

1.1 Maxwell's equations

Any thorough discussion of electromagnetism should include Maxwell's equations because they are the foundation of the subject. Maxwell's equations in differential form are given as follows:

$$\nabla \times \vec{D} = \rho_v \tag{1.1}$$

2

$$\nabla \times \vec{B} = 0 \tag{1.2}$$

$$\nabla \times \vec{E} = -\frac{\partial \vec{B}}{\partial t} \tag{1.3}$$

$$\nabla \times \vec{H} = \vec{J} + \frac{\partial \vec{D}}{\partial t} \tag{1.4}$$

$$\vec{D} = \varepsilon \vec{E} \tag{1.5}$$

$$\vec{B} = \mu \vec{H} \tag{1.6}$$

Maxwell's equations and their solutions can have application in many areas of electromagnetic research. This work focuses on three primary areas: energy transport, antenna analysis and boundary value problems (i.e. problems that are likely to be encountered in the interactions of the antenna waves), and the metamaterial slabs to be constructed later.

1.2 The wave equations

The wave equation for an electromagnetic field can be derived from Maxwell's equations.

Taking the curl of both sides of Faraday's law and Ampere's law the equations become,

$$\nabla \times \nabla \times \vec{E} = -\mu \frac{\partial}{\partial t} \left(\nabla \times \vec{H} \right) \tag{1.7}$$

$$\nabla \times \nabla \times \vec{H} = \sigma \nabla \times \vec{E} + \varepsilon \frac{\partial}{\partial t} \left(\nabla \times \vec{E} \right) \tag{1.8}$$

Substituting of eq. (1.3) into eq. (1.7) and using the identity,

$$\nabla \times \nabla \times \vec{A} = \nabla \left(\nabla \cdot \vec{A} \right) - \nabla^2 \vec{A} \tag{1.9}$$

For the left side of eq. (1.8) gives,

$$\nabla \left(\nabla \cdot \vec{E} \right) - \nabla^2 \vec{E} = -\mu \sigma \frac{\partial \vec{E}}{\partial t} - \mu \varepsilon \frac{\partial^2 \vec{E}}{\partial t^2} \tag{1.10}$$

Substitution of Gauss's Law gives,

$$\nabla^2 \vec{E} = \frac{1}{\varepsilon} \nabla \rho_v + \mu \sigma \frac{\partial \vec{E}}{\partial t} + \mu \varepsilon \frac{\partial^2 \vec{E}}{\partial t^2} \tag{1.11}$$

A similar method for eq. (1.8) yields,

$$\nabla^2 \vec{H} = \mu\sigma \frac{\partial \vec{H}}{\partial t} + \mu\varepsilon \frac{\partial^2 \vec{H}}{\partial t^2} \qquad (1.12)$$

If no sources are assumed then the eq. (1.11) and eq. (1.12) become,

$$\nabla^2 \vec{E} = \mu\varepsilon \frac{\partial^2 \vec{E}}{\partial t^2} \qquad (1.13)$$

$$\nabla^2 \vec{H} = \mu\varepsilon \frac{\partial^2 \vec{H}}{\partial t^2} \qquad (1.14)$$

These eq. (1.13) and eq. (1.14) are the vector wave equations, and can also be expressed in time-harmonic form as follows:

$$\nabla^2 \overrightarrow{E_s} = -\omega^2 \mu\varepsilon \overrightarrow{E_s} = -\beta^2 \overrightarrow{E_s} \qquad (1.15)$$

$$\nabla^2 \overrightarrow{H_s} = -\omega^2 \mu\varepsilon \overrightarrow{H_s} = -\beta^2 \overrightarrow{H_s} \qquad (1.16)$$

Where,

$$\beta^2 = -\omega^2 \mu\varepsilon \qquad (1.17)$$

1.3 Solutions to the wave equations

Solving the wave equation using separation of variables yields equations in the form,

$$f_1(x) = A_1 e^{-j\beta_x x} + B_1 e^{+j\beta_x x} \qquad (1.18)$$

$$f_2(x) = C_1 \cos(\beta_x x) + D_1 \sin(\beta_x x) \qquad (1.19)$$

Eq. (1.18) represents a traveling wave when converted from phasor form with both the incident and reflected waves, and eq. (1.19) represents a standing wave [18].

1.4 Energy carried by an electromagnetic wave

One of the main attributes of a wave is its ability to transport energy from one point to another. The power of a wave, which is the rate of energy passing a point in

4

space as a function of time, can be derived by Maxwell's equations. If eq. (1.6) is substituted into eq. (1.3) and if eq. (1.6) is substituted into eq. (1.4), the following equations result

$$\nabla \times \vec{E} = -\mu \frac{\partial \vec{H}}{\partial t} \tag{1.20}$$

$$\nabla \times \vec{H} = \sigma \vec{E} + \varepsilon \frac{\partial \vec{E}}{\partial t} \tag{1.21}$$

Taking the dot product of eq. (1.20) with $\vec{E}$ results in

$$\vec{E} \cdot \left(\nabla \times \vec{H} \right) = \sigma |E|^2 + \vec{E} \cdot \frac{\partial \vec{E}}{\partial t} \tag{1.22}$$

Using the vector identity

$$\nabla \cdot \left(\vec{A} \times \vec{B} \right) = \vec{B} \cdot \left(\nabla \times \vec{B} \right) - \vec{A} \cdot \left(\nabla \times \vec{B} \right) \tag{1.23}$$

Equation (1.22) then becomes

$$\vec{H} \cdot \left(\nabla \times \vec{E} \right) + \nabla \cdot \left(\vec{H} \times \vec{E} \right) = \sigma |E|^2 + \frac{\varepsilon}{2} \frac{\partial |E|^2}{\partial t} \tag{1.24}$$

Then taking the dot product of both sides of eq. (1.20) with $\vec{H}$ the equation becomes

$$\vec{H} \cdot \left(\nabla \times \vec{E} \right) = \vec{H} \cdot \left(-\mu \frac{\partial \vec{H}}{\partial t} \right) = -\frac{\mu}{2} \frac{\partial (|H|^2)}{\partial t} \tag{1.25}$$

Then equation (1.25) becomes

$$-\frac{\mu}{2} \frac{\partial (|H|^2)}{\partial t} - \nabla \cdot \left(\vec{E} \times \vec{H} \right) = \sigma |E|^2 + \frac{\varepsilon}{2} \frac{\partial |E|^2}{\partial t} \tag{1.26}$$

Rearranging terms and taking the integral of both sides of the equations gives

$$-\frac{\mu}{2} \frac{\partial (|H|^2)}{\partial t} - \nabla \cdot \left(\vec{E} \times \vec{H} \right) = \sigma |E|^2 + \frac{\varepsilon}{2} \frac{\partial |E|^2}{\partial t} \tag{1.27}$$

Using the divergence theorem the equation becomes

$$\int_v \nabla \cdot \left(\vec{E} \times \vec{H} \right) dv = \frac{\partial}{\partial t} \int_v \left[\frac{\varepsilon |E|^2}{2} + \frac{\mu |H|^2}{2} \right] dv - \int_v \sigma E^2 \, dv \tag{1.28}$$

Finally applying the divergence theorem to the left side gives

$$\oint_s \left(\vec{E} \times \vec{H} \right) \cdot d\vec{S} = \frac{\partial}{\partial t} \int_v \left[\frac{\varepsilon |E|^2}{2} + \frac{\mu |H|^2}{2} \right] dv - \int_v \sigma E^2 \, dv \qquad (1.29)$$

Equation (1.29) is known as *Poynting's theorem*. The right side of the side of the equations is the total power leaving a volume; the first term on the right is the rate of change in the energy stored in both the electric and magnetic fields, and the last term is the energy ohmic losses given off in heat [11]. The quantity of $\left(\vec{E} \times \vec{H} \right)$ is known as the *Poynting Vector*.

$$\vec{S} = \left(\vec{E} \times \vec{H} \right) \qquad (1.30)$$

The Poynting vector's magnitude tells how much power per unit area is leaving the volume at particular point, and the vector's direction shows the direction of the power or energy that flows out of a volume for a given electromagnetic wave [13].

1.5 Antenna analysis

This work essentially describes the interaction of an electromagnetic field from an antenna with a metamaterial lens created by embedding a high k dielectric in a low k medium. The field from the antenna structure can be generated by solving Maxwell's equations. This is usually a two step process. It is computed from magnetic vector potential $\vec{A}$ for the structure, and then the E-field is calculated. The procedure for calculating the E-field for a Hertzian dipole or a half-wavelength dipole antenna is discussed in textbooks [13, 18]. Essentially two types of fields are generated as a result of this exercise. The fields that decay at a given distance from the antenna are called evanescent fields while the fields that continue to propagate are the radiation fields. One of the functions of a metamaterial lens is to extend the near-field beyond its traditional boundary for a given antenna type. A new look into this interaction is possible by

revisiting Fresnel's formulations as applied to a metamaterial. When the angle of refraction is at the critical angle or greater between two media (i.e. there is total reflection), there are still waves that are transmitted into the second medium. These waves are referred to as evanescent waves. Evanescent waves carry no power on average and their amplitude decreases exponentially with distance. In addition, because these waves carry no power, they do not propagate [16, 19].

1.6 Snell's law and Fermat's principle

One of the major differences between ordinary materials (i.e. one with a positive refractive index), and a metamaterials is the way in which each refracts light. Therefore, an understanding of Snell's law is of great importance in studying metamaterials. Snell's law shows how a light ray refracts at the interface of two media. Fig. 1-1 shows a light ray in a medium with a refractive index of n_1 at an incident angle of θ_1 with respect to the normal of the interface, and a light ray in a medium with a refractive index of n_2 at an angle of θ_2 with respect to the normal of the interface between the two media. Snell's law is then given as:

$$\frac{\sin \theta_1}{\sin \theta_2} = \frac{n_2}{n_1} \tag{1.31}$$
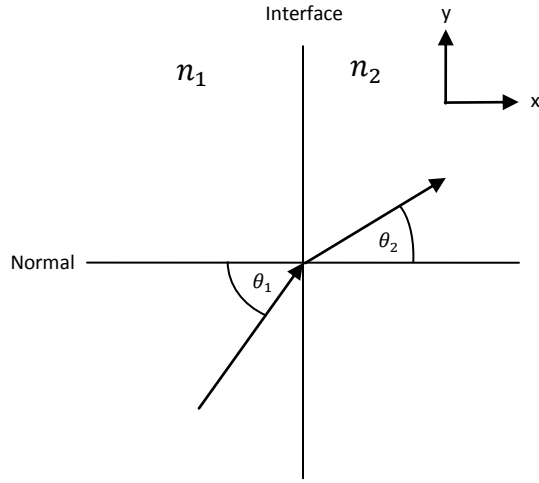
FIG. 1-1:Light ray refracting at the boundary between two mediums

Pierre de Fermat looked at light in a unique way. He stated that light would travel in the path that took the least time to complete. This is known as Fermat's principle. When looking at light from this point of view, it can be shown that the optical distance taken by light in Fig. 1-2 can be given as [20],

$$l_0 n_1 + l_i n_2 = s_0 n_1 + s_i n_2$$

(1.32)
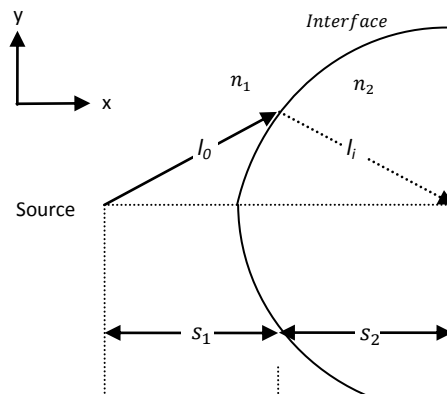
FIG. 1-2: Diagram showing terms used in Fermat's principle

This way of looking at light gives a unique insight when analyzing metamaterials as will be shown later.

1.7 Diffraction and maximum resolution

One of the major breakthroughs in the use of metamaterials was using a metamaterial lens to increase the resolution of an image. In addition, if the wavelength becomes comparable to the size of a metamaterial unit cell, then the effects of diffraction can become more pronounced. Therefore, an understanding of diffraction is of critical importance when analyzing metamaterials

In understanding about the concept of diffraction, think of the situation when observing light traveling though a flat surface with a single rectangular slit cut in it. Geometric optics would dictate the light going through the slit would have the same shape as the slit (i.e. the light would not spread out). However, this is not the case. Because of the wave nature of light, the light will not only spread out, but will also show an interference pattern. This particular phenomenon is known as diffraction. In addition, diffraction can be described as the bending of light around an object. When the object's size is comparable or smaller than the wavelength of the light, then the effects of diffraction become noticeable. One of the effects that are usually observed is a blurry image, or an image of two objects that appear as one object. However, if the information contained in the evanescent waves can be captured then the diffraction limit can be overcome.

1.8 Dispersion

Dispersion is also an essential component needed to make sense out of metamaterials, and without it the physics behind metamaterials would not work. Dispersion means the spreading out of something in this case light. This definition derives from the fact that when sunlight travels through a prism it spreads out into various colors that are electromagnetic waves of different frequencies. The reason that the colors separate in a prism is the prism itself is a dispersive material and when the

sunlight enters the prism it undergoes dispersion. Dispersion means that light at different frequencies will have different velocities when traveling through the material. The Drude model is one model that can be used to model dispersive media [8, 17]. The Drude model is given as

$$\varepsilon_r(\omega) = \varepsilon_\infty - \frac{\omega_F^2}{\omega(\omega - iv_c)} \tag{1.33}$$

where ε_∞ is the dielectric constant in the high frequency limit (i.e. $\omega \to \infty$), ω_F is the plasma frequency, and v_c is the collision frequency.

1.9 Metamaterials

In the introduction, a broad definition of metamaterial was provided, which is not the only possible definition. However, even though it is very difficult to give a short and precise definition for a metamaterial, it is easiest to think of a metamaterial as a material that is relatively homogeneous (i.e. the physical size of the material is small when compared to the wavelength of the electromagnetic wave), and that has a negative refractive index for a given frequency band [10]. Metamaterials essentially started with Veselago's famous paper entitled, *"The Electrodynamics of Substances with Simultaneously negative ϵ and μ"* where he described how metamaterials behave [1]. He gives the dispersion equation for a monochromatic wave in an isotropic media as,

$$\left|\vec{k}\right|^2 = \varepsilon\mu\omega^2 \tag{1.34}$$
$$n^2 = \varepsilon\mu \tag{1.35}$$

Maxwell's equations in phasor form are given by,

$$\nabla \times \overrightarrow{E_s} = 0 \tag{1.36}$$
$$\nabla \times \overrightarrow{H_s} = 0 \tag{1.37}$$

10

$$\nabla \times \overrightarrow{E_s} = -j\omega\mu\overrightarrow{H_s} \tag{1.38}$$

$$\nabla \times \overrightarrow{H} = (\sigma + j\omega\varepsilon)\overrightarrow{E_s} \tag{1.39}$$

$$\overrightarrow{D} = \varepsilon\overrightarrow{E} \tag{1.40}$$

$$\overrightarrow{B} = \mu\overrightarrow{H} \tag{1.41}$$

For a monochromatic plane wave the equations reduce to,

$$\vec{k} \times \overrightarrow{E} = \frac{\omega}{c}\mu\overrightarrow{H} \tag{1.42}$$

$$\vec{k} \times \overrightarrow{H} = -\frac{\omega}{c}\varepsilon\overrightarrow{E} \tag{1.43}$$

From eq. (1.42) and (1.43) changing the signs of μ and ε is the same as changing the sign of $\overrightarrow{H}$. Therefore, the Poynting vector, $(\vec{E} \times \overrightarrow{H})$, would point in the opposite direction of $\vec{k}$. This means that the energy will propagate in the opposite direction of wave propagation in the metamaterial.

Veselago showed that there must be dispersion by examining the following equation,

$$W = \varepsilon E^2 + \mu H^2 \tag{1.44}$$

He states that μ and ε cannot both be negative without the energy, W, being negative. Therefore, the equation must be rewritten in a dispersion form as follows,

$$W = \frac{\partial(\varepsilon(\omega))}{\partial\omega}E^2 + \frac{\partial(\mu(\omega))}{\partial\omega}\mu H^2 \tag{1.45}$$

In order for the energy to be positive, it is necessary for both derivatives in eq. (1.45) to be positive.

In addition the group velocity is given by,

$$\upsilon_g = \frac{d\omega(k)}{dk} \tag{1.46}$$

where $\omega(k)$ is known as the dispersion relation. If a material is non-dispersive, then the angular frequency is not a function of the wave vector. This means that a wave will have the same velocity no matter what the frequency. Therefore, eq. (1.46) would equal to the phase velocity. However, because we have already shown that a metamaterials are dispersive, then the group velocity is not necessarily the same as the phase velocity. Fig.

11

1-3 shows the direction of the group velocity and phase velocity both in free space and inside a metamaterial.
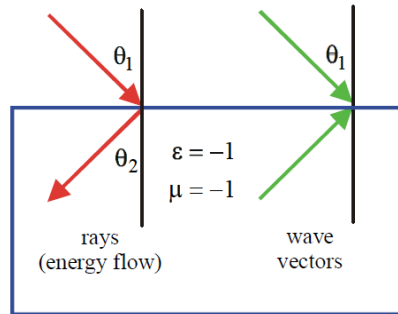
FIG. 1-3: The group velocity and phase velocity of a free space wave incident on a metamaterial [4]

1.10 Split-ring resonators (SRRs)

Veselago showed how negative refractive index materials behaved, but because there are no materials in nature that exhibit this property, the subject of metamaterials remained dormant. However, over 30 years later, a manmade material was shown to exhibit a negative refractive index. This manmade material is known as the spilt ring resonator or SRR, and it the most widely used metamaterial to date.

The first concept that is needed in order to begin understanding SRRs is the idea of homogeneity. In order to behave similarly to natural materials, the SRR unit cells should be much smaller than the wavelength of the electromagnetic wave incident on the material so that the material can be described using effective constitutive parameters (Fig. 1-4).
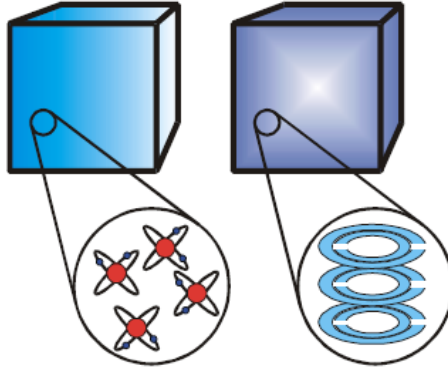
FIG. 1-4: Homogeneity in natural materials and metamaterials [4]

Even though effective constitutive parameters can be used, one of the most difficult tasks in designing SRRs or metamaterials in general is how to achieve a negative magnetic response. In order to achieve a magnetic response, a metal loop can be placed into a magnetic field, which in turn produces a current around the loop and thereby a magnetic dipole through the center of the loop. However, the sign of the magnetic response is positive. In order to make the response negative, one must change the frequency to a higher or lower frequency dependent upon which side of the resonant frequency gives the incorrect response. For example, if the operating frequency is lower than the resonant frequency and it is giving the opposite response that is needed, raise the operating frequency to a frequency that is higher than the resonant frequency and it will give the desired response. An SRR itself can be viewed as a resonant circuit, and these elements are placed at various positions away from each other to make an array such as the one shown in Fig. 1-5.
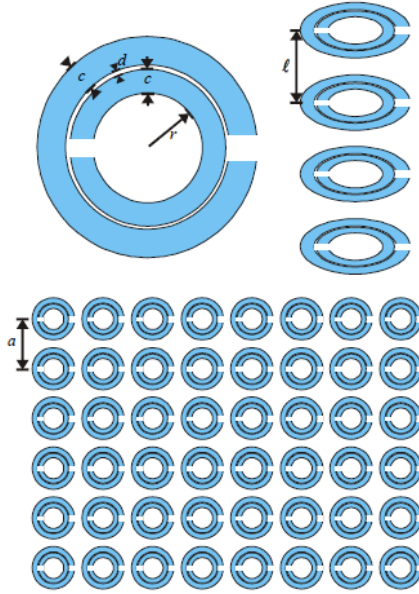
FIG. 1-5: SRR and SRR array [4]

The negative electrical response, which is more straightforward to achieve than the magnetic response, is produced by placing a metal rod behind the SRR. The rods are shown in Fig. 1-6, and an array is shown in Fig. 1-7.
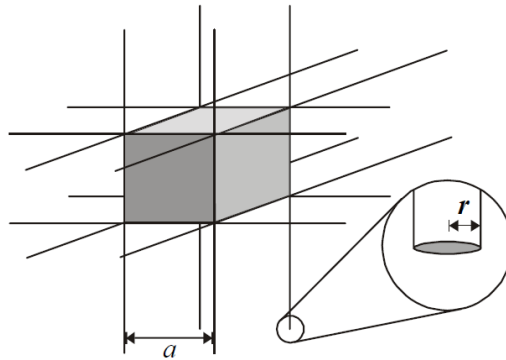
FIG. 1-6: Rods used to give negative permittivity [4]
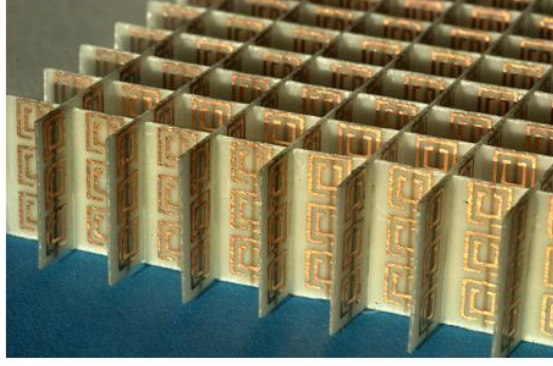
FIG. 1-7: Manufactured array of SRRs [4]

1.11 The metamaterial lens

After it was shown that actual metamaterials could be manufactured in the way of

SRRs, the path was clear to find uses of such materials. One of the uses and one of the

great discoveries in optics was the ability of a metamaterial lens to recover the near field

information that would normally be lost. This ability of a metamaterial lens to recover

the near field allows for a better resolution lens to be developed.

Pendry gives the equation,

$$\Delta \approx \frac{2\pi}{k_{max}} = \frac{2\pi c}{\omega} = \lambda \qquad (1.47)$$

as the diffraction limit of the propagating wave [5]. It is well known that if the near-field

or evanescent waves can be somehow retrieved then the diffraction limit can be

overcome. Pendry shows that this is indeed possible using a metamaterial lens [4, 5].

Pendry shows that the evanescent waves would drop off exponentially for the s-polarized

light outside of the lens as implied in the following equation:

$$\boldsymbol{E}_{1s+} = t[0,1,0]exp(ik_z'z + ik_x x - i\omega t) \qquad (1.48)$$

15

Where,

$$k_z' = +i\sqrt{k_x^2 + k_x^2 - \varepsilon\mu\omega^2 c^{-2}}, \qquad \varepsilon\mu\omega^2 c^{-2} < k_x^2 + k_y^2 \tag{1.49}$$

Pendry then derives the reflection and transmission coefficients through both sides of the metamaterial lens. First, the travelling in vacuum that is incident on the metamaterial lens has a transmission and reflection coefficient given by,

$$t' = \frac{2k_z'}{k_z' + \mu k_z}, \quad r' = \frac{k_z' - \mu k_z}{k_z' + \mu k_z} \tag{1.50}$$

Next, calculate the transmission coefficient by summing up the multiple scattering events that take place as the wave travels through the lens,

$$T_s = tt'exp(ik_z'd) + tt'r'^2exp(3ik_z'd) + tt'r'^4exp(5ik_z'd) + \cdots \tag{1.51}$$

$$= \frac{tt'exp(ik_z'd)}{1 - r'^2exp(2ik_z'd)}$$

Substitution from eq. (1.50) and taking the limit yields,

$$\lim_{\substack{\varepsilon=-1 \\ \mu=-1}} T_s = exp(-ik_zd) \tag{1.52}$$

Pendry then shows that the reflection coefficient is zero and that the similar results hold for p-polarized evanescent waves. These results show that there is no reflection from the metamaterial lens and that the metamaterial lens amplifies the evanescent waves. In addition, Maxwell's equations show that the transfer function is unity or in other words, the lens has perfect resolution. This means that all the light or information in the object plane would be transferred to the image plane. Another interesting fact is that by using Fermat's principle it can be shown that the optical distance between the object plane and the image plane is zero. Therefore, the object and the image are at the same point optically. This result means that the light rays at the object plane are the same as the light

16

rays in the image plane. How the light rays travel from the source, into the metamaterial, and then to the focal point outside the metamaterial is shown in Fig. 1-8.
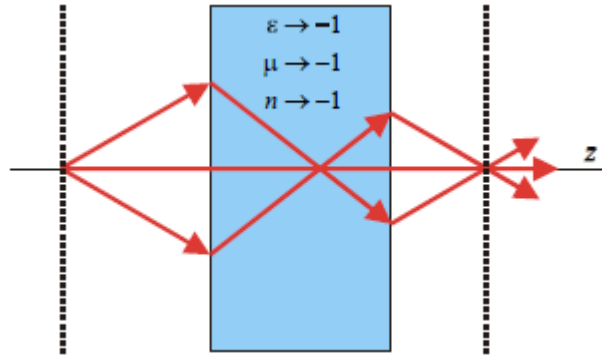
FIG. 1-8: Rays traveling from free space, into a metamaterial, and back into free space [4]

Another interesting phenomenon that Pendry discovered was that there is a mirroring effect of a wave traveling a distance *d* in free space and then traveling a distance *d* in metamaterial with a refractive index of negative one. In other words, after the wave travels through free space it seems to unravel itself as it travels through the metamaterial as shown in Fig. 1-9.
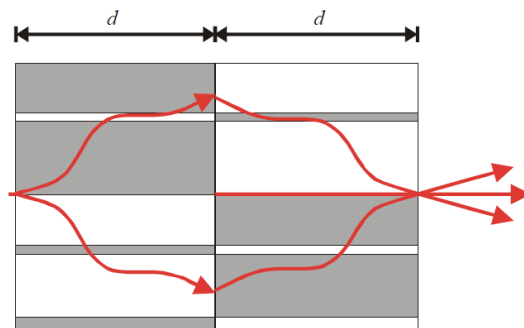
FIG. 1-9: Metamaterial mirroring effect [4]

In order to verify the theoretical results, it was necessary to construct a metamaterial lens, but this was not readily available due to the size that the lens would have to made (i.e. light is from .4µm to .7um therefore the SRR unit cell structures of the

metamaterial lens would have to be in the nanometer range). In order to get around this problem, a material with a negative ε and a positive μ was used. If the lens is placed less than a wavelength away from a surface that the light is being emitted or reflected from then there is only an electric field and no magnetic field. If there is no magnetic field, then it is possible to use a material with a positive μ in order to achieve similar results as a metamaterial. There are materials that are found in nature that have a negative ε, such as silver. This material is the one that Pendry suggested to use in order to validate the super-lens theory experimentally. The silver uses a surface resonance that is known as a surface plasmon. The silver acts as an amplifier by building up energy over time from the resonance. These resonances will build up to the point that is allowed by the silver and will not build up indefinitely due to the losses inherent in the silver. This amplification of the evanescent waves is shown in Fig. 1-10.
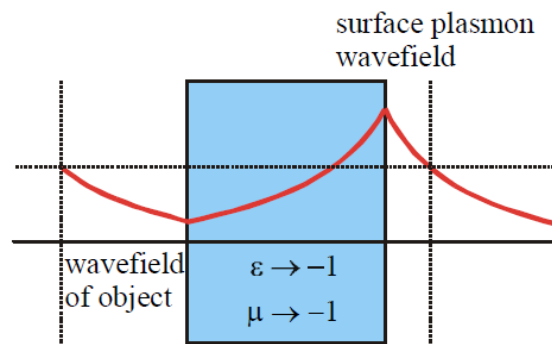
FIG. 1-10: Near-field enhancement using a metamaterial [4]

In order to achieve the surface resonance, the silver has to have a thickness of approximately one nanometer. The placement of the lens and the results are shown in Fig. 1-11.
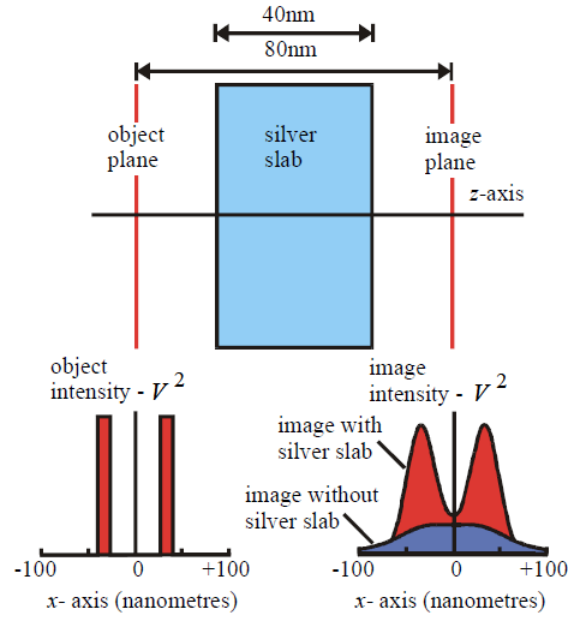
FIG. 1-11: Silver slab and image intensities [4]

It was shown that is possible to resolve both of the object's intensities and subwavelength diffraction was achieved [15]. The limiting factor of the resolution in the silver is the losses that are inherent in silver. The lower the losses of the material that is used for the lens the better the resolution. In other words, the lens acts as amplifier due to the surface resonances and the losses prevent the resonance from building up further, thereby limiting the amplification. There are materials that have less loss than silver, such as silicon carbide and it has been used in experiment to make the resolution even better [22].

CHAPTER 2

METHODS: for Designing Metamaterials

Metamaterials can be designed for a given frequency by deciding which resonator to use, what materials to use for the resonator, and the geometry of the resonator. In order to verify that metamaterial is designed properly (i.e. it will behave as a metamaterial at a given frequency), the metamaterial is constructed in CST microwave studio, ports are placed at the proper locations, and the appropriate boundary conditions are applied. Next, the structure is simulated in CST microwave studio to retrieve the s-parameters, which are then used as inputs in an algorithm that extracts the constitutive parameters from the s-parameters. The following describes the verification of the metamaterial design in more detail, and describes some issues that may arise in the design process (i.e. time dependence).

2.1 Retrieving constitutive parameters using s-parameters

One of the difficulties in metamaterial design is how to go about retrieving the value at which a structure acts as a metamaterial (i.e. the refractive index equals negative one). One such method is outlined in Smith *et al.* [2] and similarly in Chen *et al.* [3]. The process involves simulating a structure to obtain the s-parameters and using a computer algorithm to extract the constitutive parameters. A structure similar to that which Smith simulated on page 7 of his paper is shown in Fig. 2-1 below. The dimensions of the figure are given in his paper.
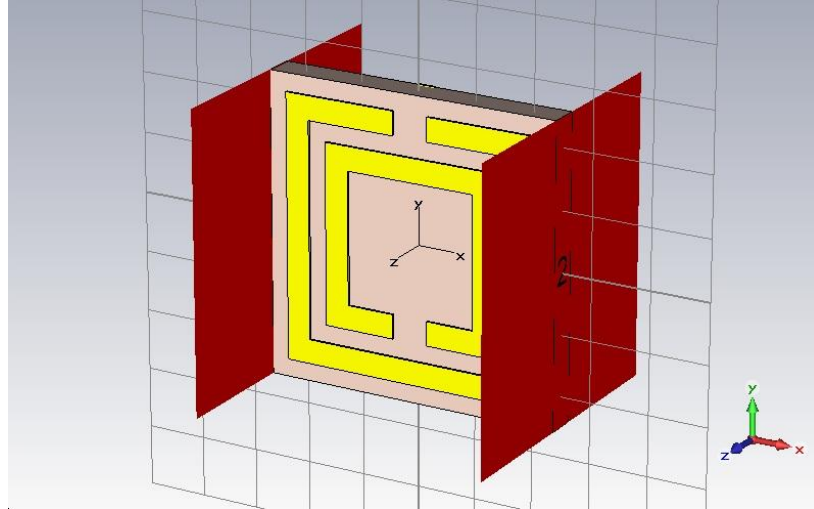
FIG. 2-1: SRR built from specifications in Smith's paper

The proper boundary conditions are necessary in order to achieve a TEM mode, which

are shown in Fig. 2-2.
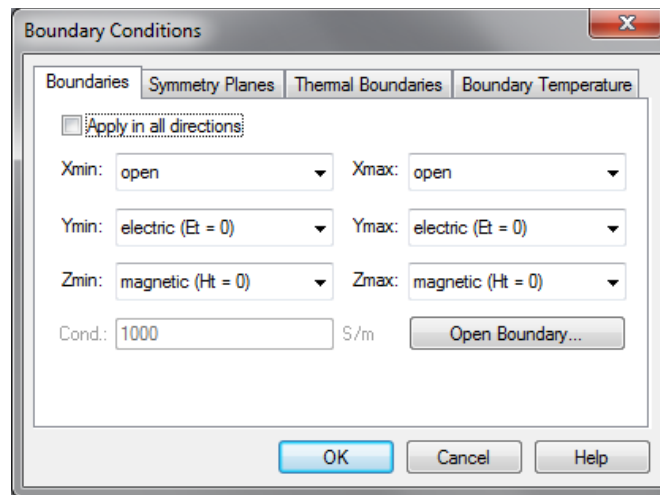
FIG. 2-2: Screenshot of boundary conditions

After the simulation is completed, the s-parameters must be exported to a text file

to be used by the algorithm in order to find the refractive index. A sample code is shown

in Appendix A, using the algorithm which is shown in the paper by Smith [1].

2.2 Results of constitutive parameter extraction algorithm with SRR

The first result is shown in Fig. 2-3; and gives the magnitude of S11 and S21, which match the results from the simulation. This result is to be expected because they are the input to the program and are therefore unchanged by the program.
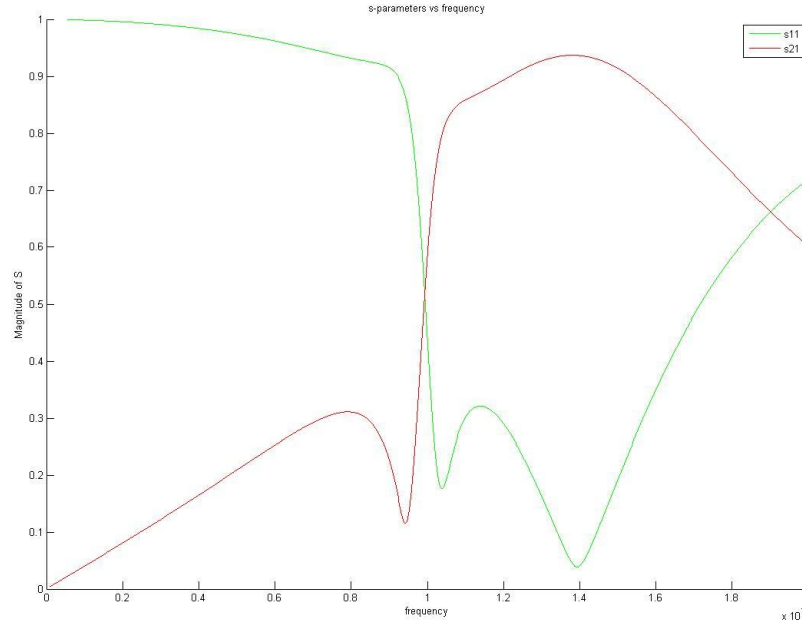
FIG. 2-3: Magnitude of s-parameters from algorithm

The next result is shown in Fig. 2-4 and is the negative of the phase given from the simulation software. The phase from the simulation results must be opposite in sign because there is a difference in the time dependence used in the simulation software and those used in the paper for deriving the equations. Therefore, the phases of S11 and S21 that are taken from the simulation results will be the negative of the phases used in the algorithm to calculate the constitutive parameters. Such issues of differences in time dependence are common when dealing with metamaterials. The results from the simulation software are also shown in Fig. 2-5.
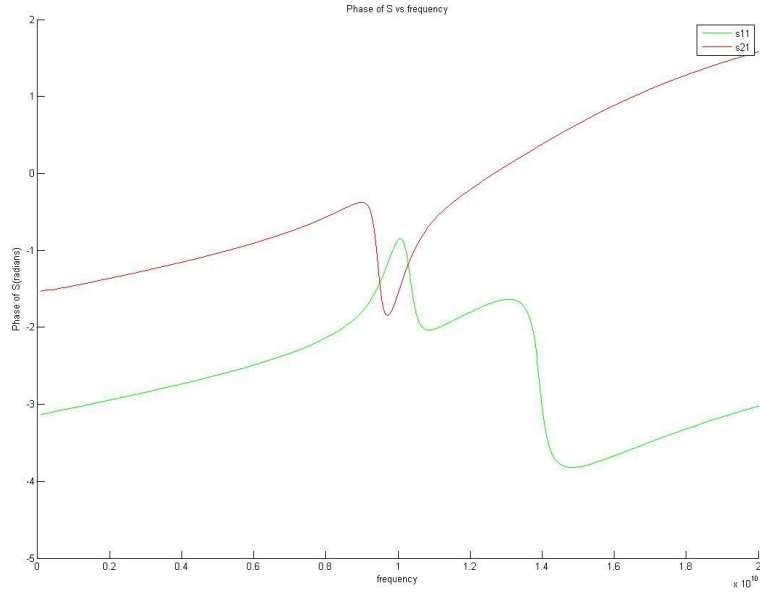
FIG. 2-4: Angles of s-parameters from algorithm
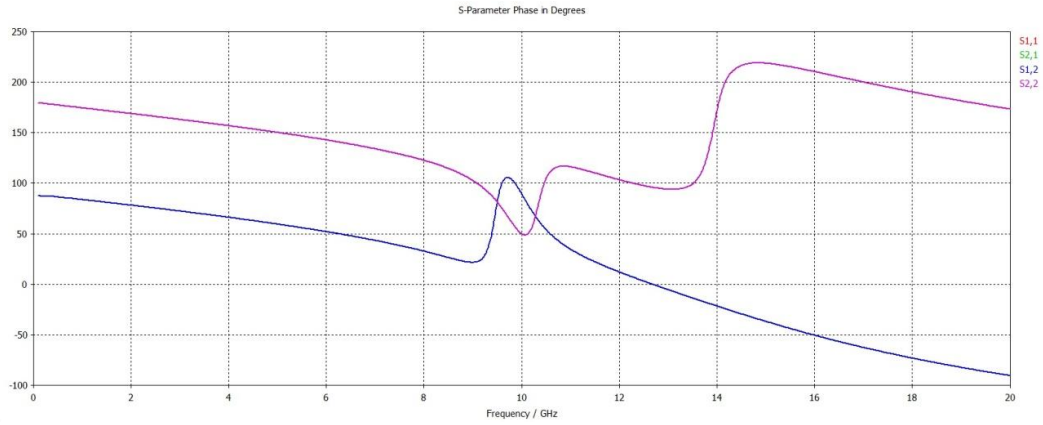
FIG. 2-5: Angles of s-parameters from simulation

The next result shown in Fig. 2-6 is the refractive index which is the most important quantity when dealing with metamaterials. The imaginary component of the refractive index is shown in red and is always positive. This is due to the constraints outlined in both the papers by Smith [2] and Chen [3]. The real component is shown in green, and it is the value with which we are most concerned. At approximately 9.274 GHz, the value of the refractive index is -1.013. This value is the frequency of concern

23

because it represents a matched case. In other words, if the wave is traveling from a material with a refractive index of one into a medium with a refractive index of negative one, then there will be no reflections. Reflections are generally undesirable because we normally want as much power as possible to be delivered from the source to the load.
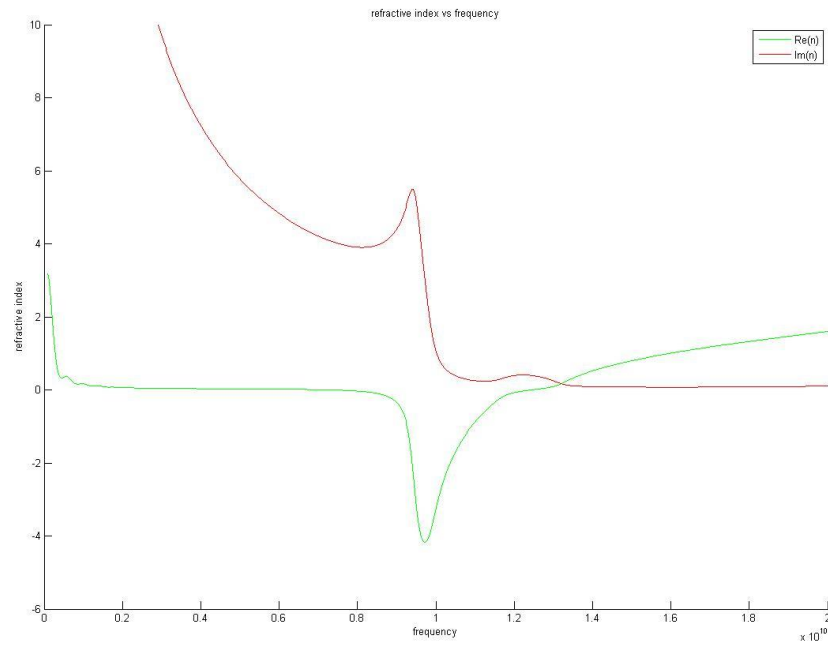
FIG. 2-6: Refractive index of the SRR from the algorithm

Next, Fig. 2-7 shows the impedance, whose values are needed to find the refractive index.
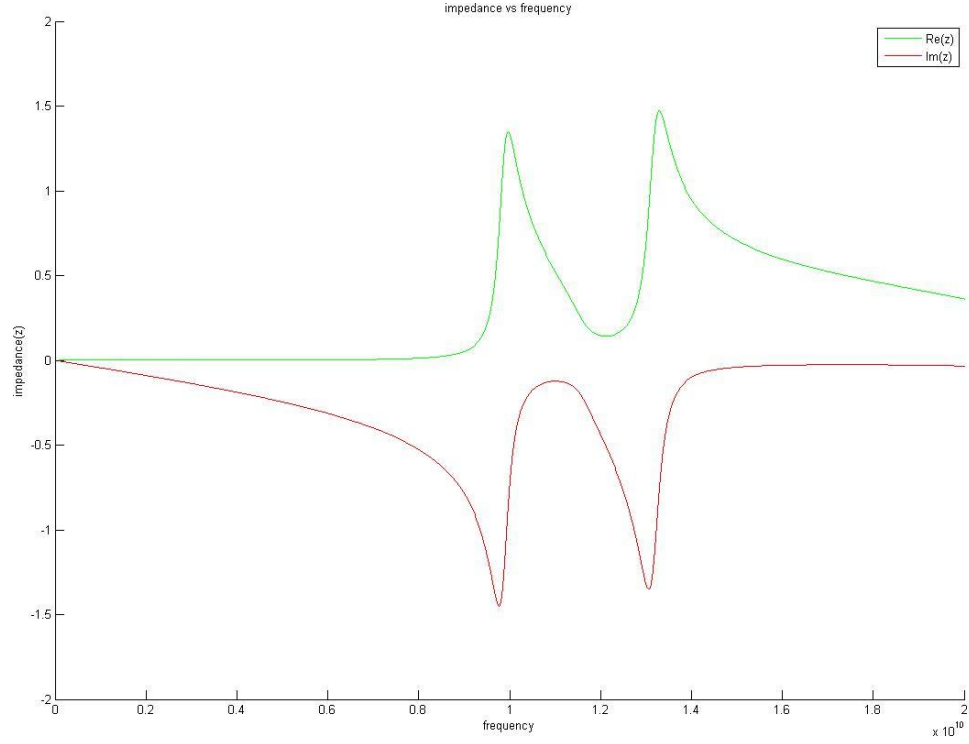
FIG. 2-7: Impedance of the SRR from the algorithm

Finally, Fig. 2-8 shows the permittivity and Fig. 2-9 shows the permeability which, when both are negative at a given frequency, results in a negative refractive index for that given frequency.
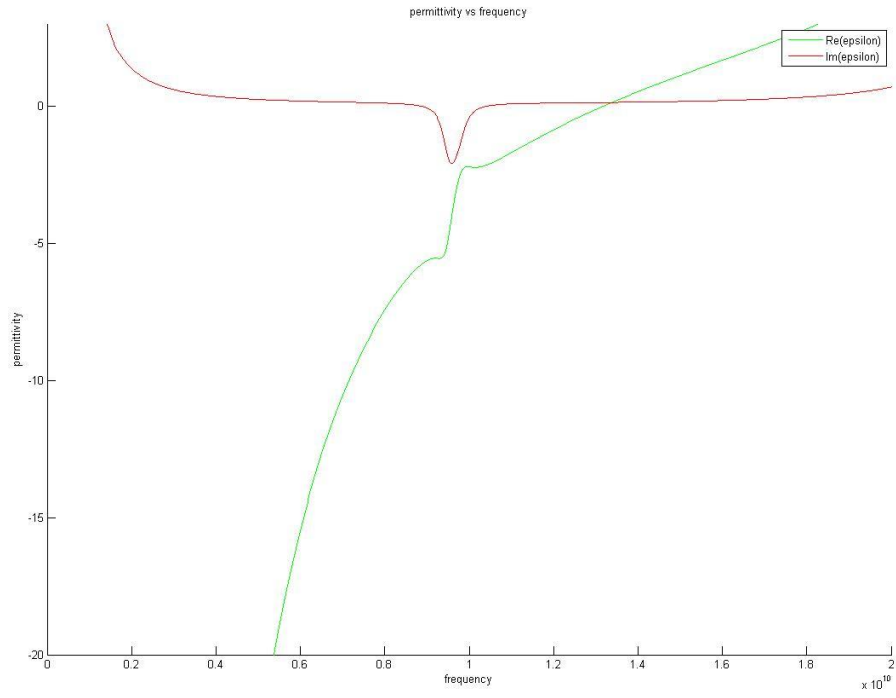
FIG. 2-8: Permittivity of the SRR from the algorithm
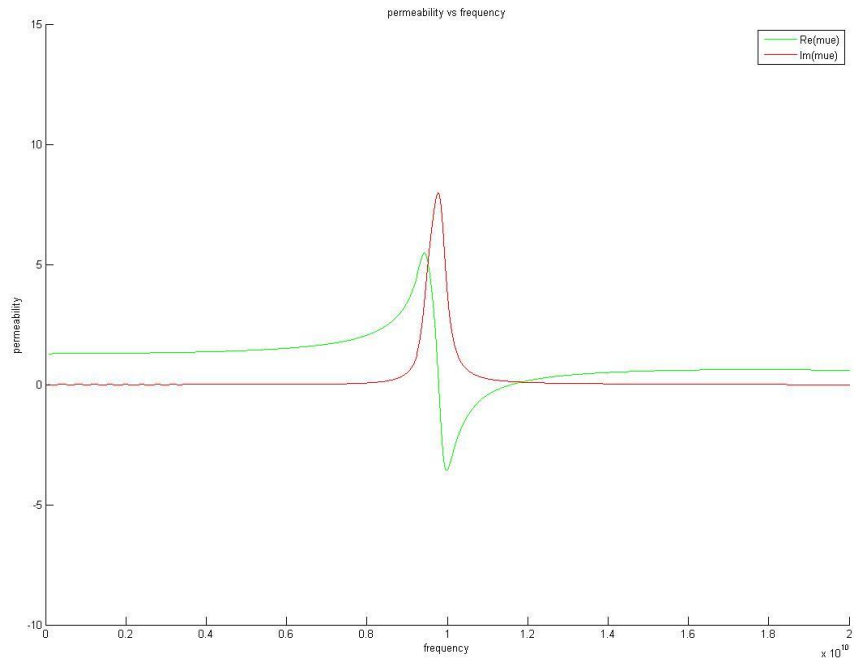
FIG. 2-9: Permeability of the SRR from the algorithm

2.3 Time-dependence differences when using metamaterials

As mentioned before, one of the common issues when dealing with metamaterials involves which time dependence to use when deriving the constitutive parameters and s-parameters. In the last section, this issue was encountered when comparing the phases from the simulation plots to the phases that were the input to the computer program (i.e. it was necessary to multiply the phases that were the output of the simulation by -1 before using it in the computer algorithm). If equations are derived using one time dependence and verified with a simulation program using the other time dependence, then the results will differ in the imaginary part. For example, the phase of the s-parameters will be the negative of the other if $e^{-j\omega t}$ is chosen for the equations, and $e^{j\omega t}$ is used by the software to calculate the s-parameters. In what follows, the constitutive parameters and s-parameters are derived first using a time dependence of $e^{j\omega t}$ and then $e^{-j\omega t}$ in order to show the effects on the imaginary components of these quantities.

Choosing a time dependence of $e^{j\omega t}$ gives a permittivity as follows [14]:

$$\vec{E}(x,y,z,t) = Re\left[\vec{E_s}(x,y,z)e^{j\omega t}\right]$$

(2.1)

$$\vec{H}(x,y,z,t) = Re\left[\vec{H_s}(x,y,z)e^{j\omega t}\right]$$

(2.2)

Using Ampere's Law

$$\nabla \times \vec{H} = \vec{J} + \varepsilon\frac{\partial \vec{E}}{\partial t}$$

(2.3)

Separating the spatial and time-dependant parts of the fields, and taking the derivative with respect to time, gives

$$\left(\nabla \times \vec{H_s}\right)e^{j\omega t} = \vec{J_s}e^{j\omega t} + \varepsilon\frac{\partial\left(\vec{E_s}e^{j\omega t}\right)}{\partial t}$$

(2.4)

$$\left(\nabla \times \overrightarrow{H_s}\right)e^{j\omega t} = \overrightarrow{J_s}e^{j\omega t} + j\omega\varepsilon\overrightarrow{E_s}e^{j\omega t} \qquad (2.5)$$

Dividing through by $e^{j\omega t}$ and using the definition of $\overrightarrow{J_s}$ gives

$$\nabla \times \overrightarrow{H_s} = \overrightarrow{J_s} + j\omega\varepsilon\overrightarrow{E_s} \qquad (2.6)$$

$$\nabla \times \overrightarrow{H_s} = \sigma\overrightarrow{E_s} + j\omega\varepsilon\overrightarrow{E_s} \qquad (2.7)$$

Extracting $\overrightarrow{E_s}$ and $j\omega$ from the right side of the equation gives

$$\nabla \times \overrightarrow{H_s} = (\sigma + j\omega\varepsilon)\overrightarrow{E_s} \qquad (2.8)$$

$$\nabla \times \overrightarrow{H_s} = j\omega\left(\varepsilon - j\frac{\sigma}{\omega}\right)\overrightarrow{E_s} \qquad (2.9)$$

The complex permittivity is then defined as:

$$\varepsilon_c = \varepsilon - j\frac{\sigma}{\omega} = \varepsilon' - j\varepsilon'' \qquad (2.10)$$

Therefore,

$$\nabla \times \overrightarrow{H_s} = j\omega\varepsilon_c\overrightarrow{E_s} \qquad (2.11)$$

Choosing a time dependence of $e^{-j\omega t}$ gives a permittivity as follows:

$$\overrightarrow{E}(x, y, z, t) = Re\left[\overrightarrow{E_s}(x, y, z)e^{-j\omega t}\right] \qquad (2.12)$$

$$\overrightarrow{H}(x, y, z, t) = Re\left[\overrightarrow{H_s}(x, y, z)e^{-j\omega t}\right] \qquad (2.13)$$

Using Ampere's Law,

$$\nabla \times \overrightarrow{H} = \overrightarrow{J} + \varepsilon\frac{\partial\overrightarrow{E}}{\partial t} \qquad (2.14)$$

and separating the spatial and time dependent parts of the fields, and taking the derivative with respect to time, gives

28

$$\left(\nabla \times \overrightarrow{H_s}\right)e^{-j\omega t} = \vec{J}_s e^{-j\omega t} + \varepsilon \frac{\partial \left(\overrightarrow{E_s}e^{-j\omega t}\right)}{\partial t} \tag{2.15}$$

$$\left(\nabla \times \overrightarrow{H_s}\right)e^{-j\omega t} = \overrightarrow{J_s}e^{-j\omega t} - j\omega\varepsilon\overrightarrow{E_s}e^{-j\omega t} \tag{2.16}$$

Dividing through by $e^{j\omega t}$ and using the definition of $\vec{J}_s$ gives

$$\nabla \times \overrightarrow{H_s} = \overrightarrow{J_s} - j\omega\varepsilon\overrightarrow{E_s} \tag{2.17}$$

$$\nabla \times \overrightarrow{H_s} = \sigma\overrightarrow{E_s} - j\omega\varepsilon\overrightarrow{E_s} \tag{2.18}$$

Extracting $\overrightarrow{E_s}$ and $j\omega$ from the right side of eq. (2.18) gives.

$$\nabla \times \overrightarrow{H_s} = (\sigma - j\omega\varepsilon)\overrightarrow{E_s} \tag{2.19}$$

$$\nabla \times \overrightarrow{H_s} = -j\omega\left(\varepsilon + j\frac{\sigma}{\omega}\right)\overrightarrow{E_s} \tag{2.20}$$

The complex permittivity is then defined as:

$$\varepsilon_c = \varepsilon + j\frac{\sigma}{\omega} = \varepsilon' + j\varepsilon'' \tag{2.21}$$

Therefore,

$$\nabla \times \overrightarrow{H_s} = -j\omega\varepsilon_c\overrightarrow{E_s} \tag{2.22}$$

Thus, the only difference between eq. (2.10) and eq. (2.21) is that the imaginary part of eq. (2.10) has the opposite sign of the imaginary part in eq. (2.21). Choosing a time dependence of $e^{j\omega t}$ gives a permeability as follows:

First, separating the spatial and time dependent parts of the fields, and taking the derivative with respect to time, gives

$$\overrightarrow{H} = \overrightarrow{H_s}e^{j\omega t} \tag{2.23}$$

$$\overrightarrow{B} = \overrightarrow{B_s}e^{j\omega t} \tag{2.24}$$

Dividing $\vec{B}$ by $\vec{H}$, gives

$$\mu = \frac{\overrightarrow{\boldsymbol{B}}}{\overrightarrow{\boldsymbol{H}}} = \frac{\overrightarrow{\boldsymbol{B}_s}e^{j(\omega t - \delta)}}{\overrightarrow{\boldsymbol{H}_s}e^{j\omega t}} = \frac{\overrightarrow{\boldsymbol{B}_s}e^{-j\delta}}{\overrightarrow{\boldsymbol{H}_s}} \qquad (2.25)$$

The complex permeability is defined as

$$\mu_c = \frac{\overrightarrow{\boldsymbol{B}_s}}{\overrightarrow{\boldsymbol{H}_s}}\cos\delta - j\frac{\overrightarrow{\boldsymbol{B}_s}}{\overrightarrow{\boldsymbol{H}_s}}\sin\delta = \mu' - j\mu'' \qquad (2.26)$$

Choosing a time dependence of $e^{-j\omega t}$ gives a permeability as follows:

$$\overrightarrow{H} = \overrightarrow{H_s}e^{-j\omega t} \qquad (2.27)$$

$$\overrightarrow{B} = \overrightarrow{B_s}e^{-j\omega t} \qquad (2.28)$$

Dividing $\overrightarrow{B}$ by $\overrightarrow{H}$ gives

$$\mu = \frac{\overrightarrow{\boldsymbol{B}}}{\overrightarrow{\boldsymbol{H}}} = \frac{\overrightarrow{\boldsymbol{B}_s}e^{-j(\omega t - \delta)}}{\overrightarrow{\boldsymbol{H}_s}e^{-j\omega t}} = \frac{\overrightarrow{\boldsymbol{B}_s}e^{j\delta}}{\overrightarrow{\boldsymbol{H}_s}} \qquad (2.29)$$

The complex permeability is

$$\mu_c = \frac{\overrightarrow{\boldsymbol{B}_s}}{\overrightarrow{\boldsymbol{H}_s}}\cos\delta + j\frac{\overrightarrow{\boldsymbol{B}_s}}{\overrightarrow{\boldsymbol{H}_s}}\sin\delta = \mu' + j\mu'' \qquad (2.30)$$

where $\tan\delta = \frac{\mu''}{\mu'}$ is the loss tangent.

Thus, the only difference between eq. (2.26) and eq. (2.30) is that the imaginary part of eq. (2.26) has the opposite sign of the imaginary part in eq. (2.30).

So, it has been shown that the choice of the time dependence of Maxwell's equations changes the sign of the imaginary component of the permittivity and permeability. Next, it will be shown that the s-parameters' imaginary component is also affected by the choice in time dependence.

The intrinsic impedance η, the reflection coefficient, and the transmission coefficient at the boundary are given by:

$$\eta = \sqrt{\frac{\mu}{\varepsilon}} \tag{2.31}$$

$$\Gamma^b = \frac{\eta_2 - \eta_1}{\eta_2 + \eta_1} \tag{2.32}$$

$$T^b = \frac{2\eta_2}{\eta_2 + \eta_1} \tag{2.33}$$

Substituting the value of $\sqrt{\frac{\mu}{\varepsilon}}$ for η, and choosing a time dependence of $e^{j\omega t}$ gives,

$$\Gamma^b = \frac{\sqrt{\dfrac{\mu_2}{\varepsilon_2}} - \sqrt{\dfrac{\mu_1}{\varepsilon_1}}}{\sqrt{\dfrac{\mu_2}{\varepsilon_2}} + \sqrt{\dfrac{\mu_1}{\varepsilon_1}}} \tag{2.34}$$

$$\Gamma^b = \frac{\dfrac{|\mu_2|^{1/2}e^{j\frac{\theta_{\mu_2}}{2}}}{|\varepsilon_2|^{1/2}e^{j\frac{\theta_{\varepsilon_2}}{2}}} - \dfrac{|\mu_1|^{1/2}e^{j\frac{\theta_{\mu_1}}{2}}}{|\varepsilon_1|^{1/2}e^{j\frac{\theta_{\varepsilon_1}}{2}}}}{\dfrac{|\mu_2|^{1/2}e^{j\frac{\theta_{\mu_2}}{2}}}{|\varepsilon_2|^{1/2}e^{j\frac{\theta_{\varepsilon_2}}{2}}} + \dfrac{|\mu_1|^{1/2}e^{j\frac{\theta_{\mu_1}}{2}}}{|\varepsilon_1|^{1/2}e^{j\frac{\theta_{\varepsilon_1}}{2}}}} \tag{2.35}$$

Equation (2.35) reduces to

$$\Gamma^b = \frac{\left(\dfrac{|\mu_2|}{|\varepsilon_2|}\right)^{1/2} e^{j/2(\theta_{\mu_2} - \theta_{\varepsilon_2})} - \left(\dfrac{|\mu_1|}{|\varepsilon_1|}\right)^{1/2} e^{j/2(\theta_{\mu_1} - \theta_{\varepsilon_1})}}{\left(\dfrac{|\mu_2|}{|\varepsilon_2|}\right)^{1/2} e^{j/2(\theta_{\mu_2} - \theta_{\varepsilon_2})} + \left(\dfrac{|\mu_1|}{|\varepsilon_1|}\right)^{1/2} e^{j/2(\theta_{\mu_1} - \theta_{\varepsilon_1})}} \tag{2.36}$$

Using Euler's formula yields

$$\Gamma^b = \frac{\left(\frac{|\mu_2|}{|\varepsilon_2|}\right)^{1/2} \cos\left(\frac{\theta_{\mu_2} - \theta_{\varepsilon_2}}{2}\right) + j\left(\frac{|\mu_2|}{|\varepsilon_2|}\right)^{1/2} \sin\left(\frac{\theta_{\mu_2} - \theta_{\varepsilon_2}}{2}\right) - \left(\frac{|\mu_1|}{|\varepsilon_1|}\right)^{1/2} \cos\left(\frac{\theta_{\mu_1} - \theta_{\varepsilon_1}}{2}\right) - j\left(\frac{|\mu_1|}{|\varepsilon_1|}\right)^{1/2} \sin\left(\frac{\theta_{\mu_1} - \theta_{\varepsilon_1}}{2}\right)}{\left(\frac{|\mu_2|}{|\varepsilon_2|}\right)^{1/2} \cos\left(\frac{\theta_{\mu_2} - \theta_{\varepsilon_2}}{2}\right) + j\left(\frac{|\mu_2|}{|\varepsilon_2|}\right)^{1/2} \sin\left(\frac{\theta_{\mu_2} - \theta_{\varepsilon_2}}{2}\right) + \left(\frac{|\mu_1|}{|\varepsilon_1|}\right)^{1/2} \cos\left(\frac{\theta_{\mu_1} - \theta_{\varepsilon_1}}{2}\right) + j\left(\frac{|\mu_1|}{|\varepsilon_1|}\right)^{1/2} \sin\left(\frac{\theta_{\mu_1} - \theta_{\varepsilon_1}}{2}\right)} \tag{2.37}$$

Grouping the real and imaginary parts yields,

$$\Gamma^b = \frac{\left[\left(\frac{|\mu_2|}{|\varepsilon_2|}\right)^{1/2}\cos\left(\frac{\theta_{\mu_2}-\theta_{\varepsilon_2}}{2}\right)-\left(\frac{|\mu_1|}{|\varepsilon_1|}\right)^{1/2}\cos\left(\frac{\theta_{\mu_1}-\theta_{\varepsilon_1}}{2}\right)\right]+j\left[\left(\frac{|\mu_2|}{|\varepsilon_2|}\right)^{1/2}\sin\left(\frac{\theta_{\mu_2}-\theta_{\varepsilon_2}}{2}\right)-\left(\frac{|\mu_1|}{|\varepsilon_1|}\right)^{1/2}\sin\left(\frac{\theta_{\mu_1}-\theta_{\varepsilon_1}}{2}\right)\right]}{\left[\left(\frac{|\mu_2|}{|\varepsilon_2|}\right)^{1/2}\cos\left(\frac{\theta_{\mu_2}-\theta_{\varepsilon_2}}{2}\right)+\left(\frac{|\mu_1|}{|\varepsilon_1|}\right)^{1/2}\cos\left(\frac{\theta_{\mu_1}-\theta_{\varepsilon_1}}{2}\right)\right]+j\left[\left(\frac{|\mu_2|}{|\varepsilon_2|}\right)^{1/2}\sin\left(\frac{\theta_{\mu_2}-\theta_{\varepsilon_2}}{2}\right)+\left(\frac{|\mu_1|}{|\varepsilon_1|}\right)^{1/2}\sin\left(\frac{\theta_{\mu_1}-\theta_{\varepsilon_1}}{2}\right)\right]} \tag{2.38}$$

Next we define $a, b, c, d, e,$ and f as follows,

$$a = \left[\left(\frac{|\mu_2|}{|\varepsilon_2|}\right)^{1/2}\cos\left(\frac{\theta_{\mu_2}-\theta_{\varepsilon_2}}{2}\right)+\left(\frac{|\mu_1|}{|\varepsilon_1|}\right)^{1/2}\cos\left(\frac{\theta_{\mu_1}-\theta_{\varepsilon_1}}{2}\right)\right] \tag{2.39}$$

$$b = \left[\left(\frac{|\mu_2|}{|\varepsilon_2|}\right)^{1/2}\sin\left(\frac{\theta_{\mu_2}-\theta_{\varepsilon_2}}{2}\right)+\left(\frac{|\mu_1|}{|\varepsilon_1|}\right)^{1/2}\sin\left(\frac{\theta_{\mu_1}-\theta_{\varepsilon_1}}{2}\right)\right] \tag{2.40}$$

$$c = \left(\frac{|\mu_2|}{|\varepsilon_2|}\right)^{1/2}\cos\left(\frac{\theta_{\mu_2}-\theta_{\varepsilon_2}}{2}\right) \tag{2.41}$$

$$d = \left(\frac{|\mu_1|}{|\varepsilon_1|}\right)^{1/2}\cos\left(\frac{\theta_{\mu_1}-\theta_{\varepsilon_1}}{2}\right) \tag{2.42}$$

$$e = \left(\frac{|\mu_2|}{|\varepsilon_2|}\right)^{1/2}\sin\left(\frac{\theta_{\mu_2}-\theta_{\varepsilon_2}}{2}\right) \tag{2.43}$$

$$f = \left(\frac{|\mu_1|}{|\varepsilon_1|}\right)^{1/2}\sin\left(\frac{\theta_{\mu_1}-\theta_{\varepsilon_1}}{2}\right) \tag{2.44}$$

Then in order to make the eq. (2.38) easier to read $a, b, c, d, e,$ and f are substituted in eq.

(2.38) and the denominator is rationalized yielding

$$\Gamma^b = \frac{[(c-d)+j(e-f)]}{a+jb}\cdot\frac{a-jb}{a-jb} \tag{2.45}$$

$$\Gamma^b = \frac{a(c-d)+ja(e-f)-jb(c-d)+b(e-f)}{a^2+b^2} \tag{2.46}$$

Using the distributive principle yields

$$\Gamma^b = \frac{(ac-ad+be-bf)+jae-jaf-jbc+jbd}{a^2+b^2} \tag{2.47}$$

Grouping the real and imaginary parts yields,

$$\Gamma^b = \frac{(ac - ad + be - bf) + j(ae - af - bc + bd)}{a^2 + b^2} \tag{2.48}$$

Choosing a time dependence of $e^{-j\omega t}$ gives,

$$\Gamma^b = \frac{\left(\frac{|\mu_2|}{|\varepsilon_2|}\right)^{1/2} e^{-j/2(\theta_{\mu_2} - \theta_{\varepsilon_2})} - \left(\frac{|\mu_1|}{|\varepsilon_1|}\right)^{1/2} e^{-j/2(\theta_{\mu_1} - \theta_{\varepsilon_1})}}{\left(\frac{|\mu_2|}{|\varepsilon_2|}\right)^{1/2} e^{-j/2(\theta_{\mu_2} - \theta_{\varepsilon_2})} + \left(\frac{|\mu_1|}{|\varepsilon_1|}\right)^{1/2} e^{-j/2(\theta_{\mu_1} - \theta_{\varepsilon_1})}} \tag{2.49}$$

Using Euler's formula yields

$$\Gamma^b = \frac{\left(\frac{|\mu_2|}{|\varepsilon_2|}\right)^{1/2} \cos\left(-\frac{\theta_{\mu_2} - \theta_{\varepsilon_2}}{2}\right) + j\left(\frac{|\mu_2|}{|\varepsilon_2|}\right)^{1/2} \sin\left(-\frac{\theta_{\mu_2} - \theta_{\varepsilon_2}}{2}\right) - \left(\frac{|\mu_1|}{|\varepsilon_1|}\right)^{1/2} \cos\left(-\frac{\theta_{\mu_1} - \theta_{\varepsilon_1}}{2}\right) - j\left(\frac{|\mu_1|}{|\varepsilon_1|}\right)^{1/2} \sin\left(-\frac{\theta_{\mu_1} - \theta_{\varepsilon_1}}{2}\right)}{\left(\frac{|\mu_2|}{|\varepsilon_2|}\right)^{1/2} \cos\left(-\frac{\theta_{\mu_2} - \theta_{\varepsilon_2}}{2}\right) + j\left(\frac{|\mu_2|}{|\varepsilon_2|}\right)^{1/2} \sin\left(-\frac{\theta_{\mu_2} - \theta_{\varepsilon_2}}{2}\right) + \left(\frac{|\mu_1|}{|\varepsilon_1|}\right)^{1/2} \cos\left(-\frac{\theta_{\mu_1} - \theta_{\varepsilon_1}}{2}\right) + j\left(\frac{|\mu_1|}{|\varepsilon_1|}\right)^{1/2} \sin\left(-\frac{\theta_{\mu_1} - \theta_{\varepsilon_1}}{2}\right)} \tag{2.50}$$

Grouping the real and imaginary parts yields

$$\Gamma^b = \frac{\left[\left(\frac{|\mu_2|}{|\varepsilon_2|}\right)^{1/2} \cos\left(-\frac{\theta_{\mu_2} - \theta_{\varepsilon_2}}{2}\right) - \left(\frac{|\mu_1|}{|\varepsilon_1|}\right)^{1/2} \cos\left(-\frac{\theta_{\mu_1} - \theta_{\varepsilon_1}}{2}\right)\right] + j\left[\left(\frac{|\mu_2|}{|\varepsilon_2|}\right)^{1/2} \sin\left(-\frac{\theta_{\mu_2} - \theta_{\varepsilon_2}}{2}\right) - \left(\frac{|\mu_1|}{|\varepsilon_1|}\right)^{1/2} \sin\left(-\frac{\theta_{\mu_1} - \theta_{\varepsilon_1}}{2}\right)\right]}{\left[\left(\frac{|\mu_2|}{|\varepsilon_2|}\right)^{1/2} \cos\left(-\frac{\theta_{\mu_2} - \theta_{\varepsilon_2}}{2}\right) + \left(\frac{|\mu_1|}{|\varepsilon_1|}\right)^{1/2} \cos\left(-\frac{\theta_{\mu_1} - \theta_{\varepsilon_1}}{2}\right)\right] + j\left[\left(\frac{|\mu_2|}{|\varepsilon_2|}\right)^{1/2} \sin\left(-\frac{\theta_{\mu_2} - \theta_{\varepsilon_2}}{2}\right) + \left(\frac{|\mu_1|}{|\varepsilon_1|}\right)^{1/2} \sin\left(-\frac{\theta_{\mu_1} - \theta_{\varepsilon_1}}{2}\right)\right]} \tag{2.51}$$

Because,

$$\sin(-\theta) = -\sin(\theta) \tag{2.52}$$

$$\cos(-\theta) = \cos(\theta) \tag{2.53}$$

then eq. (2.51) becomes,

$$\Gamma^b = \frac{\left[\left(\frac{|\mu_2|}{|\varepsilon_2|}\right)^{1/2} \cos\left(\frac{\theta_{\mu_2} - \theta_{\varepsilon_2}}{2}\right) - \left(\frac{|\mu_1|}{|\varepsilon_1|}\right)^{1/2} \cos\left(\frac{\theta_{\mu_1} - \theta_{\varepsilon_1}}{2}\right)\right] + j\left[-\left(\frac{|\mu_2|}{|\varepsilon_2|}\right)^{1/2} \sin\left(\frac{\theta_{\mu_2} - \theta_{\varepsilon_2}}{2}\right) + \left(\frac{|\mu_1|}{|\varepsilon_1|}\right)^{1/2} \sin\left(\frac{\theta_{\mu_1} - \theta_{\varepsilon_1}}{2}\right)\right]}{\left[\left(\frac{|\mu_2|}{|\varepsilon_2|}\right)^{1/2} \cos\left(\frac{\theta_{\mu_2} - \theta_{\varepsilon_2}}{2}\right) + \left(\frac{|\mu_1|}{|\varepsilon_1|}\right)^{1/2} \cos\left(\frac{\theta_{\mu_1} - \theta_{\varepsilon_1}}{2}\right)\right] - j\left[\left(\frac{|\mu_2|}{|\varepsilon_2|}\right)^{1/2} \sin\left(\frac{\theta_{\mu_2} - \theta_{\varepsilon_2}}{2}\right) + \left(\frac{|\mu_1|}{|\varepsilon_1|}\right)^{1/2} \sin\left(\frac{\theta_{\mu_1} - \theta_{\varepsilon_1}}{2}\right)\right]} \tag{2.54}$$

Then in order to make eq. (2.54) easier to read $a, b, c, d, e,$ and f are substituted and the

denominator is rationalized yielding

33

$$\Gamma^b = \frac{[(c-d)+j(-e+f)]}{a-jb} \cdot \frac{a+jb}{a+jb} \tag{2.55}$$

$$\Gamma^b = \frac{a(c-d)+ja(-e+f)+jb(c-d)-b(-e+f)}{a^2+b^2} \tag{2.56}$$

Using the distributive properties yields

$$\Gamma^b = \frac{ac-ad-jae+jaf+jbc-jbd+be-bf}{a^2+b^2} \tag{2.57}$$

Grouping the real and imaginary parts yields,

$$\Gamma^b = \frac{(ac-ad+be-bf)-j(ae-af-bc+bd)}{a^2+b^2} \tag{2.58}$$

Therefore, by inspecting eq. (2.48) and eq. (2.58) it is shown that reflection coefficient

(i.e. S11 and S22) have different signs for their imaginary component depending on

which time dependency is chosen.

A similar method used for the transmission coefficient is shown as follows:

First, the definition of the transmission coefficient at the boundary is given as,

$$T^b = \frac{2\eta_2}{\eta_2+\eta_1} \tag{2.59}$$

Substituting the value of $\sqrt{\frac{\mu}{\varepsilon}}$ for η, and choosing a time dependence of $e^{j\omega t}$ gives

$$T^b = 2 \cdot \frac{\sqrt{\frac{\mu_2}{\varepsilon_2}}}{\sqrt{\frac{\mu_2}{\varepsilon_2}}+\sqrt{\frac{\mu_1}{\varepsilon_1}}} \tag{2.60}$$

$$T^b = \frac{2 \cdot \dfrac{|\mu_2|^{1/2}e^{j\frac{\theta_{\mu_2}}{2}}}{|\varepsilon_2|^{1/2}e^{j\frac{\theta_{\varepsilon_2}}{2}}}}{\dfrac{|\mu_2|^{1/2}e^{j\frac{\theta_{\mu_2}}{2}}}{|\varepsilon_2|^{1/2}e^{j\frac{\theta_{\varepsilon_2}}{2}}}+\dfrac{|\mu_1|^{1/2}e^{j\frac{\theta_{\mu_1}}{2}}}{|\varepsilon_1|^{1/2}e^{j\frac{\theta_{\varepsilon_1}}{2}}}} \tag{2.61}$$

34

Eq. (2.61) reduces to

$$T^b = \frac{2 \cdot \left(\frac{|\mu_2|}{|\varepsilon_2|}\right)^{1/2} e^{j/2(\theta_{\mu_2}-\theta_{\varepsilon_2})}}{\left(\frac{|\mu_2|}{|\varepsilon_2|}\right)^{1/2} e^{j/2(\theta_{\mu_2}-\theta_{\varepsilon_2})} + \left(\frac{|\mu_1|}{|\varepsilon_1|}\right)^{1/2} e^{j/2(\theta_{\mu_1}-\theta_{\varepsilon_1})}} \tag{2.62}$$

Using Euler's formula yields

$$T^b = \frac{2\left[\left(\frac{|\mu_2|}{|\varepsilon_2|}\right)^{1/2} \cos\left(\frac{\theta_{\mu_2}-\theta_{\varepsilon_2}}{2}\right) + j\left(\frac{|\mu_2|}{|\varepsilon_2|}\right)^{1/2} \sin\left(\frac{\theta_{\mu_2}-\theta_{\varepsilon_2}}{2}\right)\right]}{\left(\frac{|\mu_2|}{|\varepsilon_2|}\right)^{1/2} \cos\left(\frac{\theta_{\mu_2}-\theta_{\varepsilon_2}}{2}\right) + j\left(\frac{|\mu_2|}{|\varepsilon_2|}\right)^{1/2} \sin\left(\frac{\theta_{\mu_2}-\theta_{\varepsilon_2}}{2}\right) + \left(\frac{|\mu_1|}{|\varepsilon_1|}\right)^{1/2} \cos\left(\frac{\theta_{\mu_1}-\theta_{\varepsilon_1}}{2}\right) + j\left(\frac{|\mu_1|}{|\varepsilon_1|}\right)^{1/2} \sin\left(\frac{\theta_{\mu_1}-\theta_{\varepsilon_1}}{2}\right)} \tag{2.63}$$

Grouping the real and imaginary parts yields

$$T^b = \frac{2\left[\left(\frac{|\mu_2|}{|\varepsilon_2|}\right)^{1/2} \cos\left(\frac{\theta_{\mu_2}-\theta_{\varepsilon_2}}{2}\right)\right] + 2j\left[\left(\frac{|\mu_2|}{|\varepsilon_2|}\right)^{1/2} \sin\left(\frac{\theta_{\mu_2}-\theta_{\varepsilon_2}}{2}\right)\right]}{\left[\left(\frac{|\mu_2|}{|\varepsilon_2|}\right)^{1/2} \cos\left(\frac{\theta_{\mu_2}-\theta_{\varepsilon_2}}{2}\right) + \left(\frac{|\mu_1|}{|\varepsilon_1|}\right)^{1/2} \cos\left(\frac{\theta_{\mu_1}-\theta_{\varepsilon_1}}{2}\right)\right] + j\left[\left(\frac{|\mu_2|}{|\varepsilon_2|}\right)^{1/2} \sin\left(\frac{\theta_{\mu_2}-\theta_{\varepsilon_2}}{2}\right) + \left(\frac{|\mu_1|}{|\varepsilon_1|}\right)^{1/2} \sin\left(\frac{\theta_{\mu_1}-\theta_{\varepsilon_1}}{2}\right)\right]} \tag{2.64}$$

Next we define a, b, c, d, e, and f as follows

$$a = \left[\left(\frac{|\mu_2|}{|\varepsilon_2|}\right)^{1/2} \cos\left(\frac{\theta_{\mu_2}-\theta_{\varepsilon_2}}{2}\right) + \left(\frac{|\mu_1|}{|\varepsilon_1|}\right)^{1/2} \cos\left(\frac{\theta_{\mu_1}-\theta_{\varepsilon_1}}{2}\right)\right] \tag{2.65}$$

$$b = \left[\left(\frac{|\mu_2|}{|\varepsilon_2|}\right)^{1/2} \sin\left(\frac{\theta_{\mu_2}-\theta_{\varepsilon_2}}{2}\right) + \left(\frac{|\mu_1|}{|\varepsilon_1|}\right)^{1/2} \sin\left(\frac{\theta_{\mu_1}-\theta_{\varepsilon_1}}{2}\right)\right] \tag{2.66}$$

$$c = 2 \cdot \left(\frac{|\mu_2|}{|\varepsilon_2|}\right)^{1/2} \cos\left(\frac{\theta_{\mu_2}-\theta_{\varepsilon_2}}{2}\right) \tag{2.67}$$

$$d = 2 \cdot \left(\frac{|\mu_2|}{|\varepsilon_2|}\right)^{1/2} \sin\left(\frac{\theta_{\mu_2}-\theta_{\varepsilon_2}}{2}\right) \tag{2.68}$$

In order to make eq. (2.64) easier to read, a, b, c, and d are substituted in equation and the denominator is rationalized yielding

$$T^b = \frac{c + jd}{a + jb} \cdot \frac{a - jb}{a - jb} \tag{2.69}$$

35

Using the distributive properties yields

$$T^b = \frac{ac + jad - jbc + bd}{a^2 + b^2}$$

(2.70)

Grouping the real and imaginary parts yields

$$T^b = \frac{ac + bd + j(ad - bc)}{a^2 + b^2}$$

(2.71)

Next, chose a time dependence of $e^{-j\omega t}$ which gives

$$T^b = \frac{2 \cdot \left(\frac{|\mu_2|}{|\varepsilon_2|}\right)^{1/2} e^{-j/2(\theta_{\mu_2} - \theta_{\varepsilon_2})}}{\left(\frac{|\mu_2|}{|\varepsilon_2|}\right)^{1/2} e^{-j/2(\theta_{\mu_2} - \theta_{\varepsilon_2})} + \left(\frac{|\mu_1|}{|\varepsilon_1|}\right)^{1/2} e^{-j/2(\theta_{\mu_1} - \theta_{\varepsilon_1})}}$$

(2.72)

Using Euler's formula yields

$$T^b = \frac{2\left[\left(\frac{|\mu_2|}{|\varepsilon_2|}\right)^{1/2} \cos\left(-\frac{\theta_{\mu_2} - \theta_{\varepsilon_2}}{2}\right)\right] + 2j\left[\left(\frac{|\mu_2|}{|\varepsilon_2|}\right)^{1/2} \sin\left(-\frac{\theta_{\mu_2} - \theta_{\varepsilon_2}}{2}\right)\right]}{\left[\left(\frac{|\mu_2|}{|\varepsilon_2|}\right)^{1/2} \cos\left(-\frac{\theta_{\mu_2} - \theta_{\varepsilon_2}}{2}\right) + \left(\frac{|\mu_1|}{|\varepsilon_1|}\right)^{1/2} \cos\left(-\frac{\theta_{\mu_1} - \theta_{\varepsilon_1}}{2}\right)\right] + j\left[\left(\frac{|\mu_2|}{|\varepsilon_2|}\right)^{1/2} \sin\left(-\frac{\theta_{\mu_2} - \theta_{\varepsilon_2}}{2}\right) + \left(\frac{|\mu_1|}{|\varepsilon_1|}\right)^{1/2} \sin\left(-\frac{\theta_{\mu_1} - \theta_{\varepsilon_1}}{2}\right)\right]}$$

(2.73)

Because

$$\sin(-\theta) = -\sin(\theta)$$

(2.74)

$$\cos(-\theta) = \cos(\theta)$$

(2.75)

then eq. (2.73) becomes

$$T^b = \frac{2\left[\left(\frac{|\mu_2|}{|\varepsilon_2|}\right)^{1/2} \cos\left(\frac{\theta_{\mu_2} - \theta_{\varepsilon_2}}{2}\right)\right] - 2j\left[\left(\frac{|\mu_2|}{|\varepsilon_2|}\right)^{1/2} \sin\left(\frac{\theta_{\mu_2} - \theta_{\varepsilon_2}}{2}\right)\right]}{\left[\left(\frac{|\mu_2|}{|\varepsilon_2|}\right)^{1/2} \cos\left(\frac{\theta_{\mu_2} - \theta_{\varepsilon_2}}{2}\right) + \left(\frac{|\mu_1|}{|\varepsilon_1|}\right)^{1/2} \cos\left(\frac{\theta_{\mu_1} - \theta_{\varepsilon_1}}{2}\right)\right] - j\left[\left(\frac{|\mu_2|}{|\varepsilon_2|}\right)^{1/2} \sin\left(\frac{\theta_{\mu_2} - \theta_{\varepsilon_2}}{2}\right) + \left(\frac{|\mu_1|}{|\varepsilon_1|}\right)^{1/2} \sin\left(\frac{\theta_{\mu_1} - \theta_{\varepsilon_1}}{2}\right)\right]}$$

(2.76)

In order to make the eq. (2.76) easier to read, $a, b, c,$ and d are substituted and the denominator is rationalized yielding

$$T^b = \frac{c - jd}{a - jb} \cdot \frac{a + jb}{a + jb} \qquad (2.77)$$

Using the distributive properties yields,

$$T^b = \frac{ac - jad + jbc + bd}{a^2 + b^2} \qquad (2.78)$$

Grouping the real and imaginary parts yields,

$$T^b = \frac{(ac + bd) - j(ad - bc)}{a^2 + b^2} \qquad (2.79)$$

Therefore, by inspecting eq. (2.71) and eq. (2.79) it is shown that reflection coefficient (i.e. S21 and S12) have different signs for their imaginary component depending on which time dependence is chosen.

2.4 Metamaterial lens filter and gain enhancement

There have been a number of papers recently that have used metamaterials for gain enhancement. One example is in the paper by Weng *et al.* [23], where a metamaterial is placed in front of a fractal patch antenna as shown in Fig. 2-10.
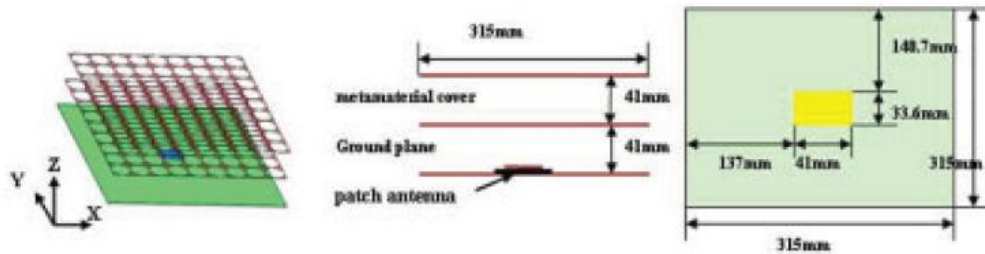

FIG. 2-10: Metamaterial with patch antenna [21]

37

The unit cells of the array were square shaped with a circle cut out of the center as shown in Fig. 2-11.
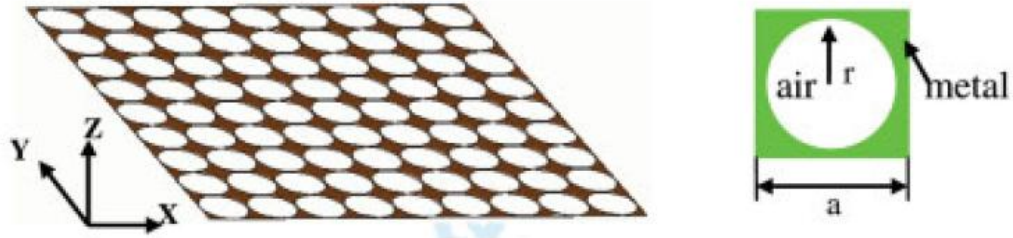

FIG. 2-11: Metamaterial array [21]

The operating frequency was 2.55 GHz. There was dramatic improvement in the gain (i.e. from 7.4 to 17.4dB) when the metamaterial was placed in front of the antenna. The 2D plots for the results are shown in Fig. 2-12 and the 3D plots are shown in Fig. 2-13.
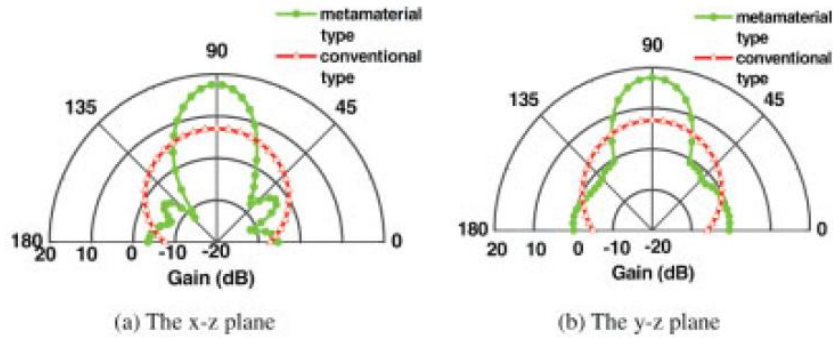

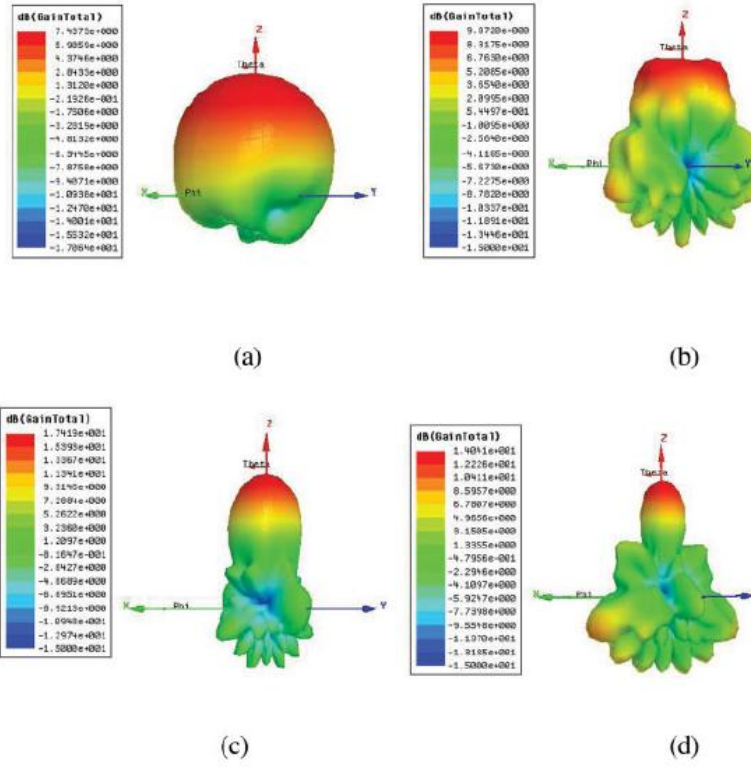**FIG. 2-12: 2D radiation patterns at 2.55 GHz [21]**

FIG. 2-13: 3D radiation patterns at 2.55 GHz [21]

In another example taken from a paper by Wu *et al.* [23], a metamaterial was placed in front of a horn antenna as shown in Fig. 2-14.
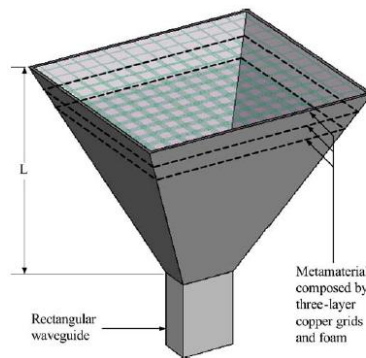

FIG. 2-14: Horn antenna with metamaterial [23]

The unit cells of the array were square shaped with squares cut out of the centers shown in Fig. 2-15.
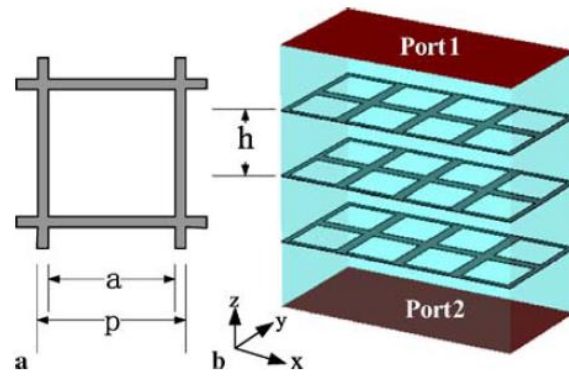
FIG. 2-15: Metamaterial array [23]

Again there was some improvement in the gain (i.e. from a maximum of 18.33 dB to a maximum of 20.74 dB) when the metamaterial was placed in front of the antenna. The 2D radiation results for the e-field plane and h-field plane are shown in Fig. 2-16.
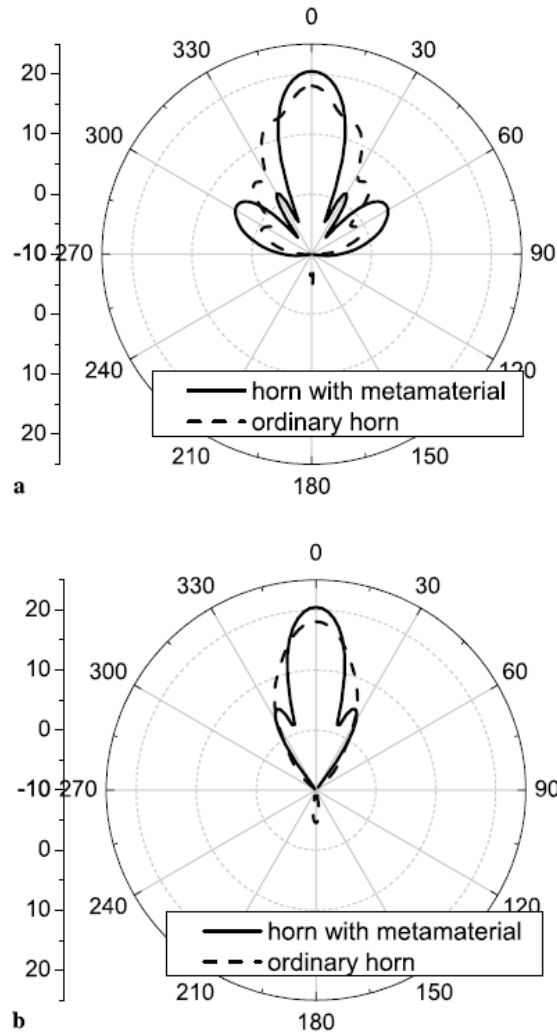
FIG. 2-16: Radiation pattern at 16.40 GHz [23]

2.5 CHDR based metamaterial and lens

Although it has been shown when using the previously mentioned metamaterials a significant gain results, their use may not be applicable in a high power application. However, there are resonators that exhibit qualities that make them suitable for high power applications. One such resonator is the cubic high dielectric resonator or CHDR.

Using the computer algorithm presented earlier, a metamaterial in the form of a slab will be designed. The slab chosen is called a cubic high dielectric resonator (CHDR) similar to the CHDR in the paper by J. Kwon and A. Gopinath [12], and it is shown in Fig. 2-17.
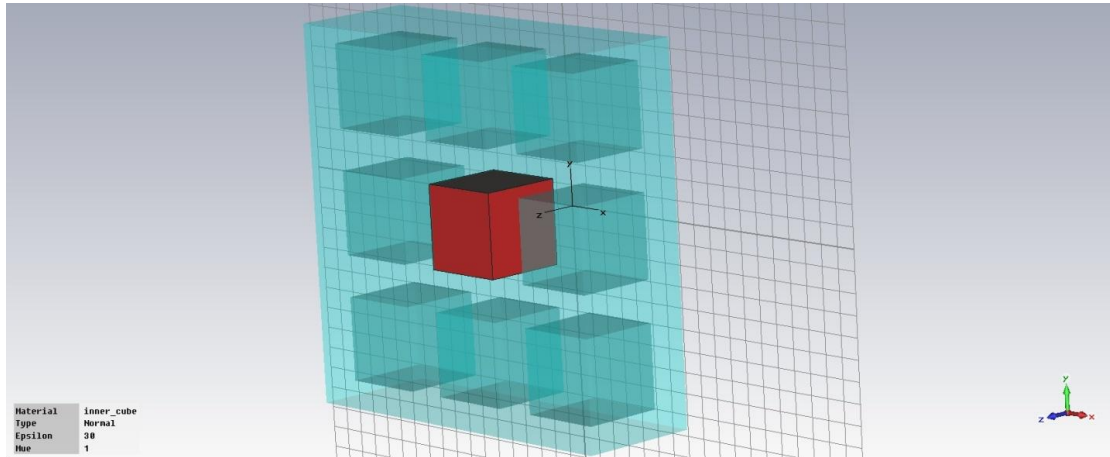

Material	inner_cube
Type	Normal
Epsilon	30
Mue	1

FIG. 2-17: CHDR metamaterial used in simulation

2.6 Refractive index for CHDR

The CHDR was simulated using waveguide ports, and the s-parameters were exported and used as inputs to the computer program in order to retrieve the refractive index as a function of frequency. The Fig. 2-18 shows the refractive index of the CHDR using the computer algorithm.
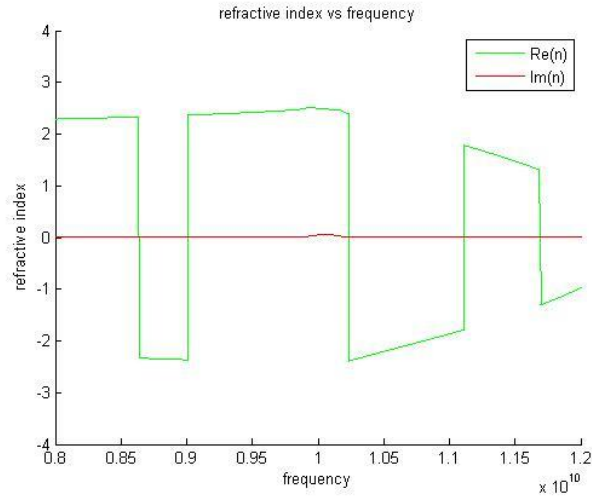
FIG. 2-18: Refractive index of CHDR as a function of frequency

For a frequency of 10.4 GHz the results show a negative refractive index. However, this is not the ideal case, because the refractive index appears to be around negative two. Therefore, reflections will cause the angle of refraction at the interface between free space and the metamaterial will be different than the ideal case. Even with these drawbacks, it will be shown that this choice in metamaterial will allow for gain enhancement.

2.7 Antennas used in simulations

Antennas are extremely important in electronics. The main purpose of an antenna is to act as a transducer by transforming a guided wave into a free space wave, doing so as efficiently as possible. One example of an antenna that is widely used is a patch antenna. Patch antennas are widely used due to their low profile (i.e. ability to fit into certain electronics), and are relatively easy to design and manufacture. One special type of a patch antenna is a fractal patch antenna. Fractal patch antennas are a better choice in electronics applications where miniaturization is paramount. A fractal patch antenna

43

gives the same resonant frequency as other patch antennas, but can have a smaller

physical size for the same resonant frequency.   Another important attribute of

antennas besides efficiency is directivity, which is the focusing of the radiating energy.

Using these two concepts together gives the gain of the antenna. In this paper,

metamaterials are used with patch antennas in order to increase the antennas gain.

There were two antennas that were used as electromagnetic sources during the

simulations. For one set of simulations, a circular patch antenna with a resonant

frequency of 10.4 GHZ was used; and, for the other set of simulations, a fractal patch

antenna with a resonant frequency of 10.4 GHz was used. The circular patch antenna is

shown in Fig. 2-19. The radius of the circular patch is 5.5 mm, with a dielectric substrate

($\varepsilon = 2.08$) of 13.5 x 13.5 x 1.2 mm, and a ground plane of 13.5 x 13.5 mm. The thickness

of all metal components defined as perfect electric conductors, is 0.001mm.
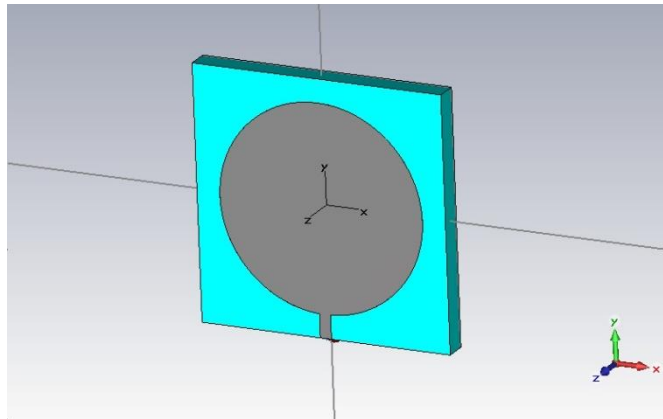

FIG. 2-19: Circular patch antenna used in simulations

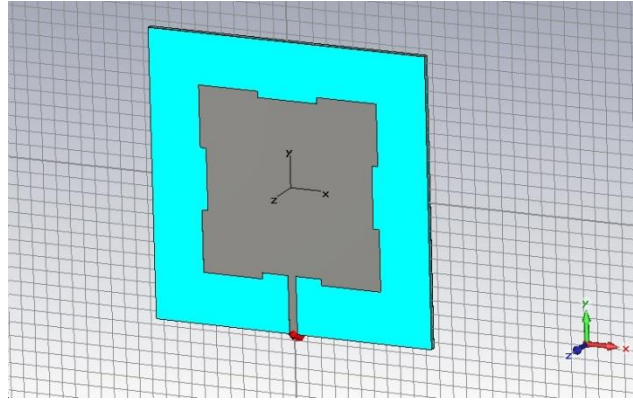The fractal patch antenna [9] designed for 10.4 GHz is shown in Fig. 2-20.

FIG. 2-20: Fractal patch antenna used in simulations

2.8 Introduction to modeling of metamaterial lenses

This section will explore how one can construct a metamaterial in order to achieve maximum gain enhancement; and using this explanation, it will be shown how both extending the near-field and the refraction of electromagnetic rays help achieve this goal.

First an antenna, designed to obtain a directive broadside far-field pattern at 10.4 GHz, was placed a certain distance away from a metamaterial lens (meta-lens). The metamaterial lens that was used was a homogenous structure which implemented the Drude model to calculate both a permittivity and permeability of -1 at 10.4 GHz. The device was simulated using the finite-difference time-domain method (FDTD) with the magnitude of the near-zone electric field (E-field) being calculated from the steady-state phasors obtained through discrete Fourier transforms (DFTs) of the time-domain samples (i.e., CST microwave studio).

In the past, there have been a wide variety of lens shapes that have been explored using right-handed materials such as glass. For example, light rays can be bent by a lens so that they converge to a second focal point. Therefore, the light located at the object plane should be identical to that of the light of the image plane. Unfortunately, this is not the case due to reflection, absorption, and scattering. However, with the use of a metamaterial lens, some of these problems can be reduced and a more perfect representation of the original light rays can be reproduced.

Pendry's paper on a perfect lens [4] discusses how the diffraction limit can be overcome by the use of metamaterials. In fact, he showed that theoretically the resolution can be infinite. In his paper, a metamaterial slab was used with the light traveling through free-space, then through a metamaterial with a refractive index of -1, and then through free space again. Because the absolute values of the refractive indices are the same, there will be no reflection loss. Also, absorption can be ignored even though in practice it cannot be ignored and will affect the diffraction limit. Pendry also showed that a metamaterial acts as an amplifier in regards to the near-field, which means that we can retrieve those parts of the electromagnetic waves that would have normally died off exponentially [4, 5, 7]. Because of this phenomenon, we are able to replicate the source at a distance away from the source. With right-handed materials, the diffraction limit is on the order of one wavelength. However, we are assuming a perfectly homogeneous metamaterial with no absorption, and without reflection, so geometric optics may be used to describe the path of the electromagnetic rays.

The geometry of a lens focusing to a point is dictated by Fermat's equation [20],

$$l_0 n_1 + l_i n_2 = s_0 n_1 + s_i n_2$$

(2.80)

46

In our case, where $n_1 = -n_2$, and by making $s_0 = s_i$, eq. (2.80) then becomes,

$$l_0 - l_i = 0$$

Therefore, the length of the ray l_0 must equal the ray l_i. In addition, because $n_1 = 1$ and $n_2 = -1$, then, when the ray travels across the boundary, it will refract at angle with respect to the normal of the surface that is equal but opposite to what would have been traveled by the ray if both materials where of the same refractive index. Another interesting observation of the eq. (2.81) is that it shows that the optical distance between the source and the focal point is zero. Therefore, the source and the focal point are identical as far as the light is concerned.

In addition, to focusing the light onto one point, all the light rays can be made to point in one direction. A light ray inside a metamaterial incident on the boundary between the metamaterial and free space is shown in Fig 2-21.
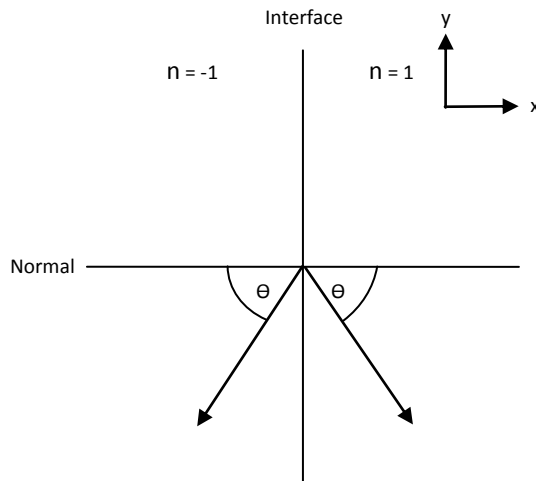

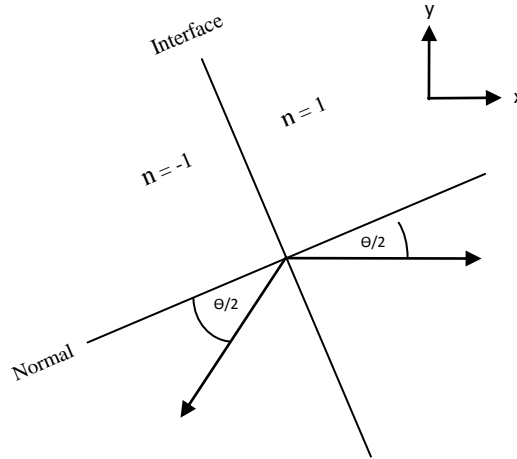**FIG. 2-21: Light ray exiting a metamaterial into free space**

**FIG. 2-22: Rotating the normal of the interface
between a metamaterial and free space**

Fig. 2-22 shows that, given an angle Θ that the ray makes with the normal from within a metamaterial, the normal can then be rotated at an angle that can redirect the ray in an arbitrary direction.

2.9 Spherical waveform and choice of metamaterial lens

Next, assume a circular waveform radiating from a point source. When a metamaterial is placed in front of the source, the rays from the source will travel from free space into the metamaterial and then back into free space. Therefore, there are two interfaces that must be considered. The first interface will focus the rays in such a way as to create a point source inside the metamaterial that is identical to the original point source, while the second interface will send the rays into the direction that we desire. For the first step in the lens design process, a flat surface will be placed a distance d away from the source with a thickness d for the first interface. The light rays will then come to a focal point d away from the first interface as shown in Fig. 2-23.
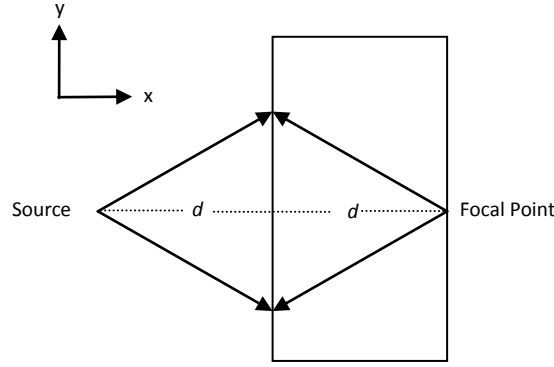
FIG. 2-23: Replicating the source inside of a metamaterial

The second interface is chosen so that the rays radiating from the focal point will be directed in the x-direction. If the second interface is first assumed to be a circle of radius r with the center at the focal point inside the metamaterial, then a ray incident upon the surface with an angle Θ would continue straight and not refract. However, if we use Fig. 2-21 and Fig. 2-22 as guides, they show that, if the normal has been rotated counter-clockwise by Θ, then it is necessary rotate the normal back clockwise by Θ/2 so that the ray will be directed in the x-direction. In other words, the tangent or slope of the interface for an incident ray of angle Θ at a distance r away from the source must be equal to the slope at the angle Θ/2 at a distance r away from the source. The surface that satisfies this condition is a parabolic lens with a focus located at the focal point inside of the metamaterial and the wavefront located at the directrix of the parabolic lens as shown in Fig. 2-24.
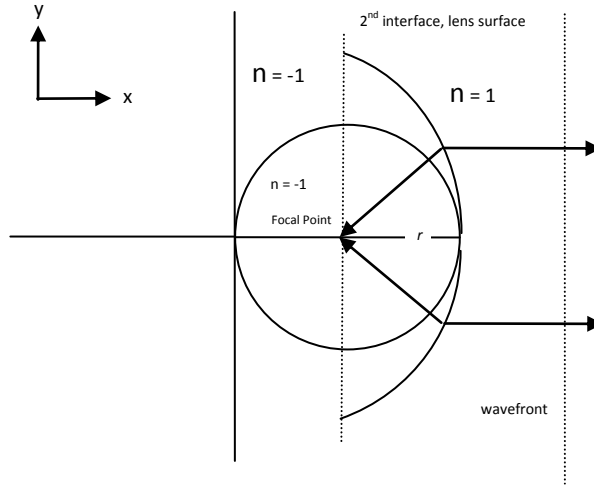
FIG. 2-24: Parabolic lens directing rays in the x-direction

This conclusion can be shown as follows. The circle has an equation in polar form as,

$r(\theta) = a$, where a is the radius of the circle. The slope of the circle at any point is given

by

$$\frac{dy}{dx} = \frac{\frac{dr}{d\theta}\sin\theta + r\cos\theta}{\frac{dr}{d\theta}\cos\theta - r\sin\theta} = -\frac{1}{\tan\theta} \qquad (2.82)$$

The parabola has an equation in polar form as

$$\frac{dy}{dx} = \frac{\frac{dr}{d\theta}\sin\theta + r\cos\theta}{\frac{dr}{d\theta}\cos\theta - r\sin\theta} = -\frac{1}{\tan\frac{\theta}{2}} \qquad (2.83)$$

where r is the distance from the focus to the vertex of the parabola. The slope of the

parabola at any point is given by

50

$$\frac{dy}{dx} = \frac{\frac{dr}{d\theta}\sin\theta + r\cos\theta}{\frac{dr}{d\theta}\cos\theta - r\sin\theta} = -\frac{1}{\tan(\frac{\theta}{2})} \tag{2.84}$$

Therefore, the slope of parabola at a given value of Θ has the same value as the slope of the circle at Θ/2. In other words, the slope of the parabola lags the slope of the circle by Θ/2. This satisfies the condition that we need in order for the light rays to be directed in the x-direction. This result can be extended to three dimensions because of the symmetry of the spherical wave source. In addition, the smaller the radius of the circle, and therefore the smaller the focus of the parabolic lens, the more directive the light rays become.

The source that was used in the simulation was a circular patch antenna. The circular patch antenna was designed to operate at 10.4 GHz. The dimensions were a 5.5 mm radius, the dielectric was 13.5 x 13.5 x 1.2 mm, the ground was 13.5x13.5 mm, and the thickness of all metal components was 0.001 mm. The dielectric was given a dielectric constant of 2.08, and the metal that was used was a perfect electric conductor. The patch antenna is shown in Fig. 2-19.

The metamaterial lens was simulated using the Drude model, allowing for a refractive index of -1 at 10.4 GHz. Eq. (2.85) and eq. (2.86) are used to calculate the correct parameters to input into the software program in order to give a refractive index of -1 at a frequency of 10.4 GHz. Fig. 2-25 shows the graph of the permittivity and permeability that is used as input to the simulation program. The block portion of the metamaterial is 100 x 100 x 10 mm, and is placed 10 mm in front of the patch antenna. The focus of the parabola was chosen to be 18 mm due to the shape of the wave from the focal point

inside the metamaterial and is placed 20 mm in front of the patch antenna. Fig. 2-26

shows the metamaterial lens used in the simulation.

$$\varepsilon_r(\omega) = \varepsilon_\infty - \frac{\omega_F^2}{\omega(\omega - iv_c)} \tag{2.85}$$

$$\mu_r(\omega) = \mu_\infty - \frac{\omega_F^2}{\omega(\omega - iv_c)} \tag{2.86}$$
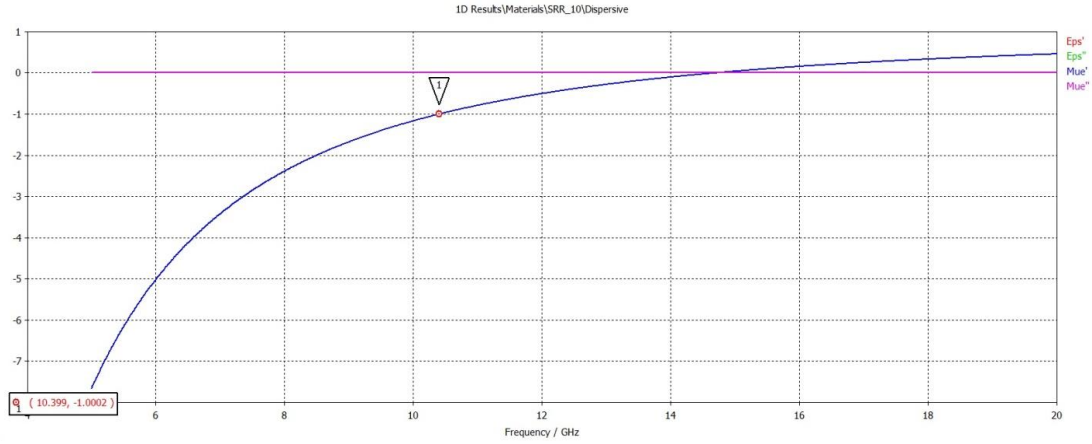

FIG. 2-25: Permittivity and permeability of metamaterial based on the Drude model
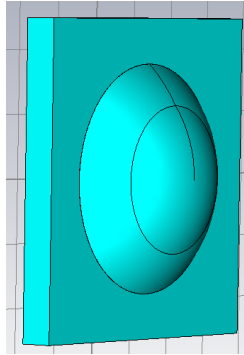

FIG. 2-26: Metamaterial lens used in simulation

2.10 Metamaterials in power applications

The reason for the choice of CHDRs over other metamaterials (i.e. Split Ring

Resonators (SRR)) is for high power applications. When placed in an electromagnetic

field, SRRs will heat up considerably more than CHDRs due to the high eddy currents that take place in the SRRs. This heating is mainly due to the low resistivity conductors used in the construction of SRRs. In comparison, the CHDR uses dielectric material with very high resistivity, causing very small eddy currents.

In order to demonstrate the benefits of using a CHDR over an SRR in high power applications, an SRR and CHDR were simulated in CST microwave studio using EM and thermal co-simulation. The SRR was constructed using the same materials as outlined in Smith's paper [1]. The dielectric of the SRR is FR-4 lossy with a dielectric constant of 3.84, and the metal used was copper. The materials used for the CHDR were Teflon for the outer cube with a dielectric constant of 2.1 and Glycerin for the inner cube with a dielectric constant of 50. Both structures are designed to have a resonance frequency of 10.4 GHz. The simulation used a power factor of 65W and a background temperature of 300K.

CHAPTER 3

RESULTS

3.1 Circular patch antenna simulation results using CHDR filter

The results are taken from the electromagnetic simulation software suite CST Microwave Studio [6].The electric field radiating from the circular patch antenna is shown in Fig. 3-1. The electric field radiates away from the antenna in a circular pattern with some back radiation.
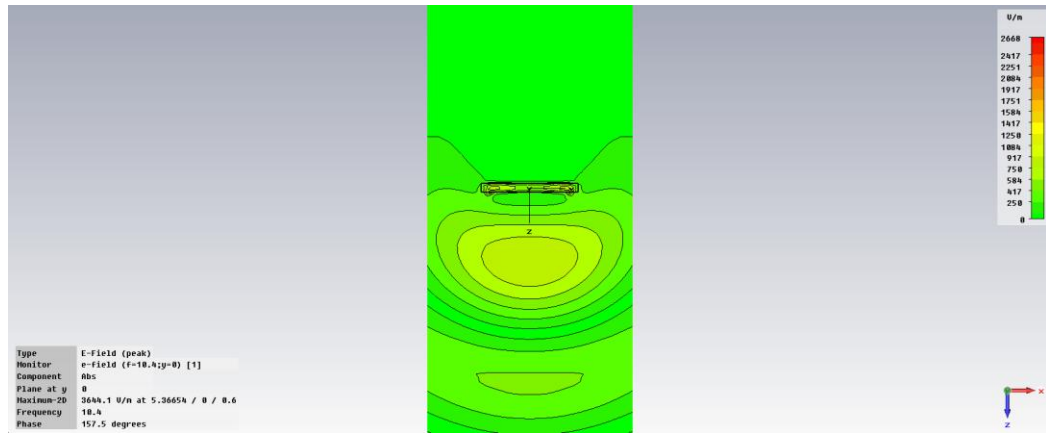

FIG. 3-1: Electric field radiating from circular patch antenna

The radiation pattern in Fig. 3-2 shows the circular patch antenna as the radiator at 10.4 GHz with a metamaterial placed in front of it.
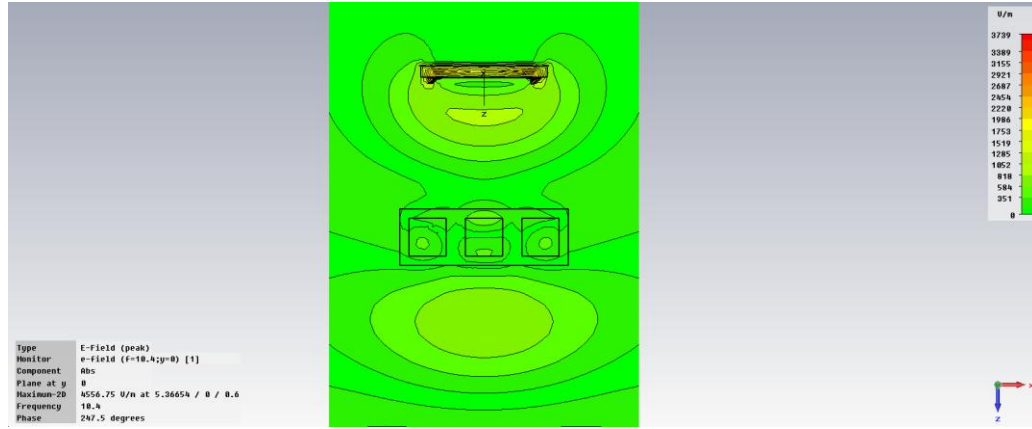

FIG. 3-2: Electric Field pattern of circular patch antenna and CHDR metamaterial filter

The Fig. 3-3 and Fig. 3-4 show the radiation pattern of the circular patch antenna both without a metamaterial filter and with the metamaterial placed at various distances in front of the antenna.
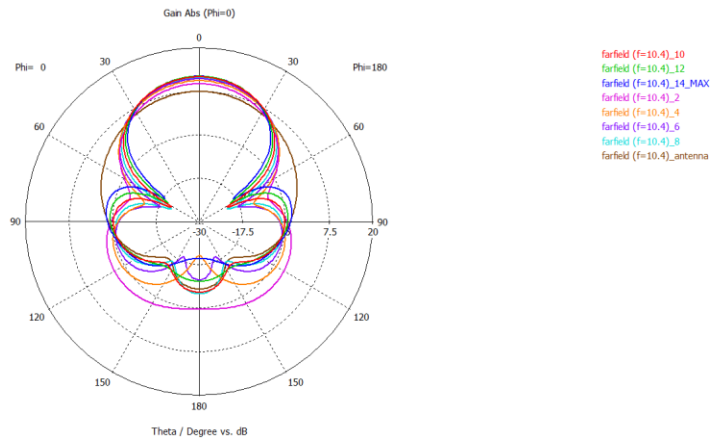

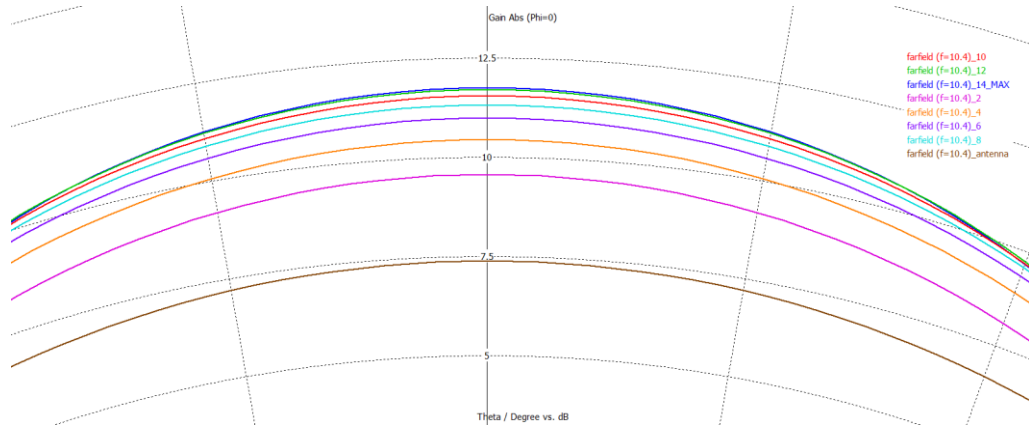**FIG. 3-3: Radiation pattern of circular patch antenna at 10.4 GHz**

Gain Abs (Phi=0)

12.5

10

7.5

5

Theta / Degree vs. dB

farfield (f=10.4)_10
farfield (f=10.4)_12
farfield (f=10.4)_14_MAX
farfield (f=10.4)_2
farfield (f=10.4)_4
farfield (f=10.4)_6
farfield (f=10.4)_8
farfield (f=10.4)_antenna

FIG. 3-4: Close up view of the radiation pattern of circular patch antenna at 10.4 GHz

3.2 Fractal patch antenna simulation results using CHDR filter

The electric field radiating from the fractal patch antenna is shown in Fig. 3-5. The electric field radiates away from the antenna in a circular pattern with some back radiation.
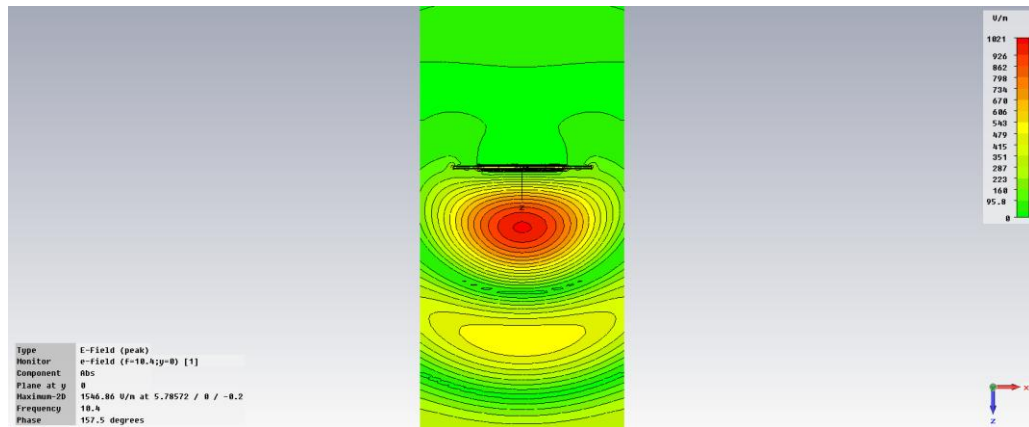

FIG. 3-5: Electric field radiating from fractal patch antenna

The radiation pattern in Fig. 3-6 shows the fractal patch antenna as the radiator at 10.4 GHz with a metamaterial placed in front of it.
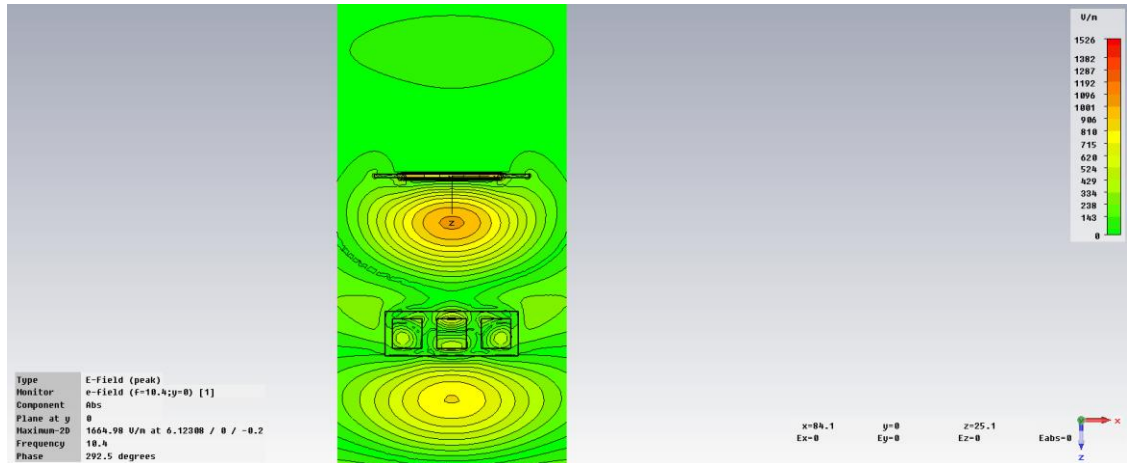
FIG. 3-6: Electric Field pattern of fractal patch antenna and CHDR metamaterial filter

Fig. 3-7 and Fig. 3-8 below show the radiation pattern for the both the fractal patch antenna only, and fractal patch antenna with the metamaterial filter placed at various distances away from the fractal antenna.
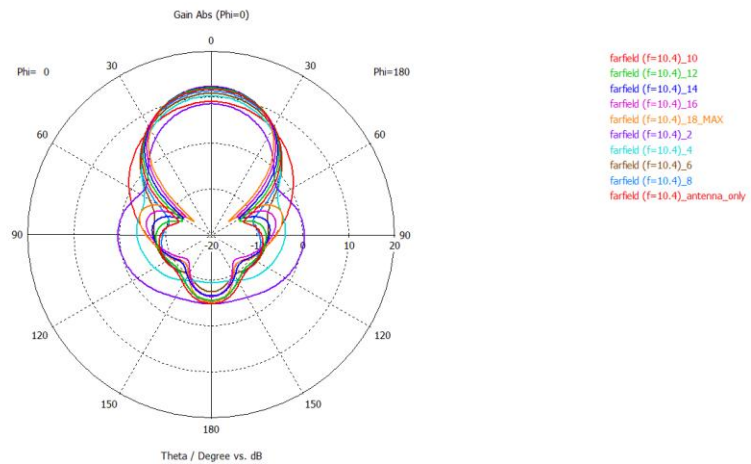

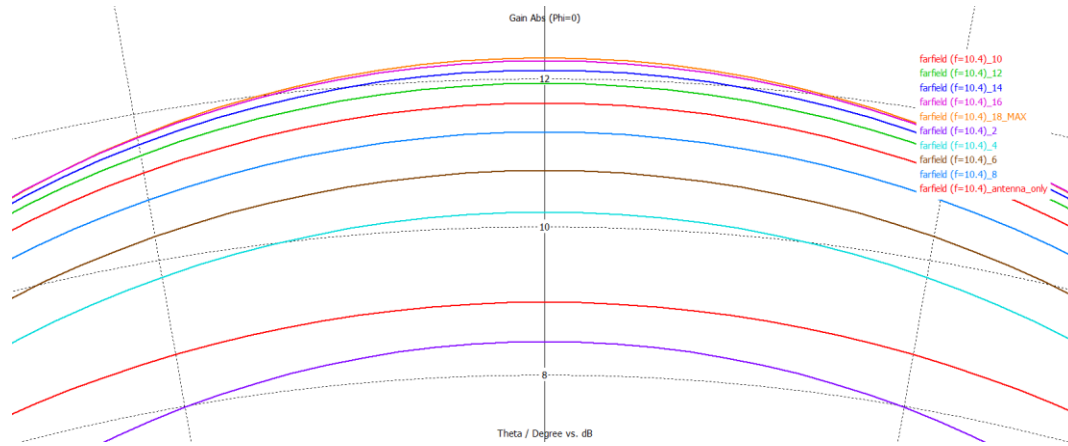**FIG. 3-7: Radiation pattern of fractal patch antenna at 10.4 GHz**

Gain Abs (Phi=0)

farfield (f=10.4)_10
farfield (f=10.4)_12
farfield (f=10.4)_14
farfield (f=10.4)_16
farfield (f=10.4)_18_MAX
farfield (f=10.4)_2
farfield (f=10.4)_4
farfield (f=10.4)_6
farfield (f=10.4)_8
farfield (f=10.4)_antenna_only

Theta / Degree vs. dB

FIG. 3-8: Close up view of the radiation pattern of fractal patch antenna at 10.4 GHz

3.3 Simulation results using Drude model metamaterial lens

The concept presented in Sections 2.7 and 2.8 can be demonstrated through simulations using an algorithm for simulating dispersive media [3], specifically the Drude media simulation technique incorporated in an electromagnetic simulation software suite [2].

Fig. 3-9 shows the slab portion of the homogeneous metamaterial lens, and the electric field at 10.4 GHz. Notice how the electric field of the slab is showing a mirroring effect.
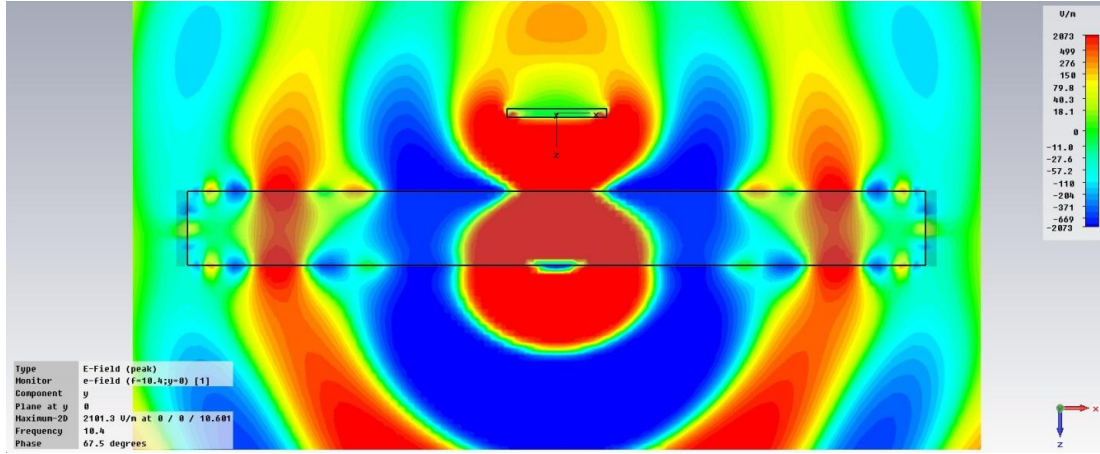
FIG. 3-9: Metamaterial slab portion of the lens and the e-field mirroring effect

Fig. 3-10 shows the antenna with the metamaterial lens. Notice that the electric field in front of the lens starts to resemble a plane wave.
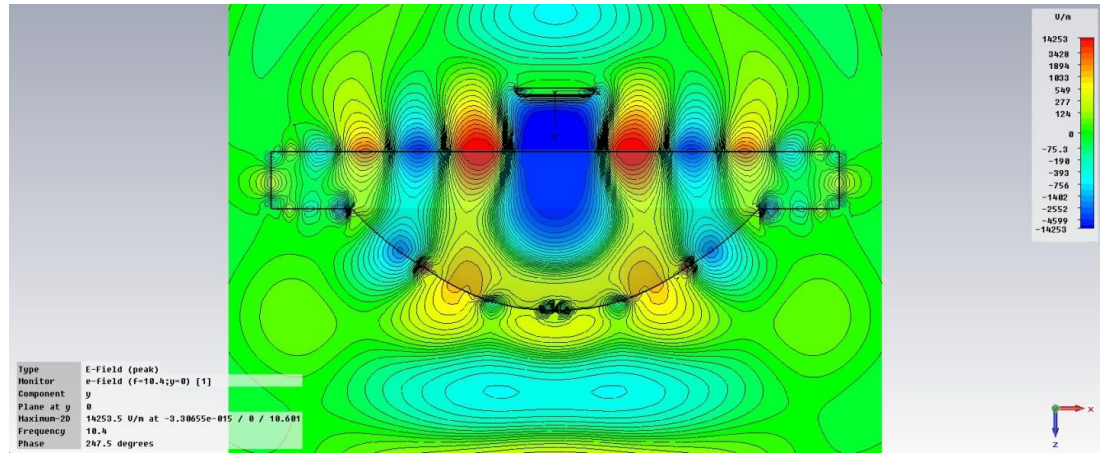

FIG. 3-10: Circular patch antenna with metamaterial lens

Fig. 3-11 shows the 2D radiation pattern for the circular patch antenna and the circular antenna with the metamaterial lens. The green plot is radiation pattern of the circular patch antenna without the metamaterial lens, and the red plot is the radiation pattern with the metamaterial lens.
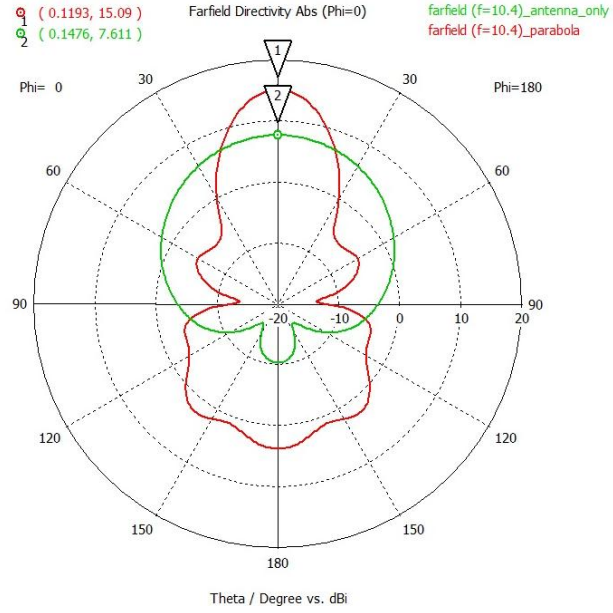
FIG. 3-11: 2D radiation pattern for circular patch antenna only and with metamaterial lens at 10.4 GHz

The 3D radiation pattern for the circular patch antenna only is shown in Fig. 3-12, and the 3D radiation pattern for the circular patch antenna with the metamaterial lens in shown in Fig 3-13.
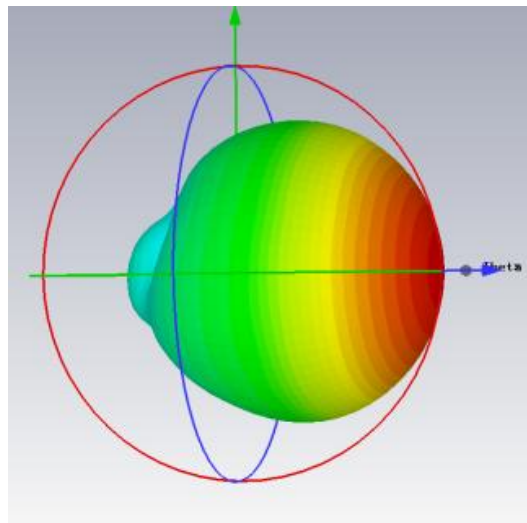
FIG. 3-12: 3D radiation pattern for circular patch antenna only at 10.4 GHz
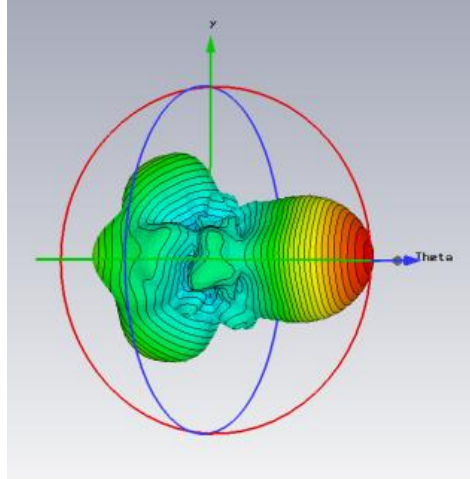
FIG. 3-13: 3D radiation pattern for circular patch antenna with metamaterial lens at 10.4 GHz

3.4 Thermal simulation results for SRR and CHDR

The results of the simulation show that part of the SRR structure (Fig. 3-14) heated up to a maximum 1676 K, whereas part of the CHDR structure (3-15) only heated up to a maximum of 300.16K.

FIG. 3-14: Temperature simulation of SRR

FIG. 3-15: Temperature simulation of CHDR

CHAPTER 4

DISCUSSION

When the metamaterial filter was used in conjunction with an antenna, the gain was improved. Using the CHDR metamaterial filter enhances the near-field and thereby extends the source. In addition, the metamaterial refracts the electromagnetic rays in such a wa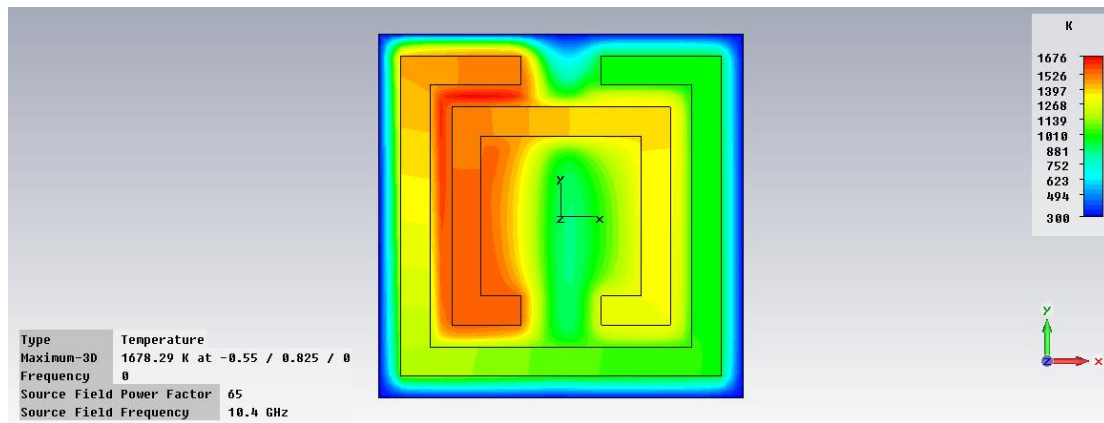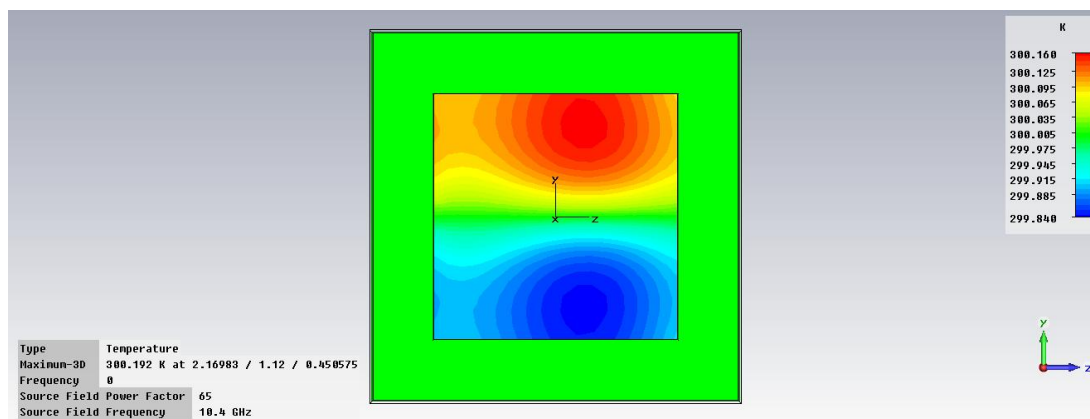y that improves the directivity.   This feature is shown in the radiation pattern Fig. 3-3 with a circular patch antenna as the radiator at 10.4 GHz.   Also, Fig. 3-2 shows that the near-field is extended and that the electromagnetic waves were refracted in such a way as to improve the gain. For the circular patch antenna, the optimum placement of the CHDR metamaterial filter is 14 mm away from the source, and the gain improvement for the circular patch antenna was from 7.383 dB to 11.75 dB. Fig. 3-7 shows the radiation pattern for the fractal patch antenna and the metamaterial filter, with the filter placed at various distances away from the fractal antenna. As before, Fig. 3-6 shows that the near-field is extended, and it also shows that the electromagnetic rays are refracted in such a way as to improve the gain of the antenna when using a CHDR metamaterial filter. The maximum gain improvement for the fractal patch antenna and CHDR metamaterial filter combination occurs when the filter is placed approximately 18 mm in front of the fractal antenna, and the gain improvement for the fractal patch antenna was from 8.984 dB to 12.28 dB.

The homogenous metamaterial lens that used the Drude dispersion model also showed improvement. With the use of the homogeneous metamaterial lens, the directivity was increase considerably from a maximum of   7.611 dBi without a meta-lens to 15.09 dBi with a meta-lens as shown in Fig. 3-11. Also, the gain was increased from a

63

maximum of 7.382 dB without the meta-lens to a maximum of 12.11 dB with the meta-lens. It is also showed an increase in the back lobes of the radiation pattern, which may be due to the source not emitting a perfect spherical wave and thereby causing more complex refractions of the waves. However, it is clearly evident by the three-dimensional wave patterns that the wave becomes much more directive with the use of a meta-lens as shown in Fig. 3-13.

Finally, the results of the simulation show that part of the SRR structure heated up to a maximum 1676K (Fig. 3-14), whereas part of the CHDR structure only heated up to a maximum of 300.16K (Fig. 3-15). This result clearly demonstrates the benefit of using a CHDR for high power applications.

CHAPTER 5

CONCLUSION

It has been shown that if a metamaterial lens was placed in front of an antenna (i.e. a fractal patch antenna or a circle patch antenna) that the gain is improved. In addition, it was shown that there does exist an optimum distance to place the metamaterial in front of the lens to allow for maximum gain enhancement. Moreover, a theory has been presented on how to create a metamaterial lens in order to direct electromagnetic rays in a direction of our choosing. In particular, a spherical wave radiating from a point source was chosen and the rays were directed in one direction in order to improve the gain. In the simulation, a fractal patch antenna was used as a source radiating at 10.4 GHz, and a meta-lens with a refractive index of negative one at 10.4 GHz. The simulation agreed strongly with the theory that was presented showing a significant increase in directivity from 7.611dBi to 15.09dBi with the use of the meta-lens. Also, the gain was improved from 7.382dB to 12.11dB with the use of the meta-lens. Finally, the CHDR was used in place of the SRR because of the thermal performance of the CHDR compared to the SRR when both were subjected to an electromagnetic wave of equal power.

The next step would be design and simulate an SRR or CHDR metamaterial in the shape of the homogeneous metamaterial lens rather than using just a slab. Clearly, the simulation results for the homogeneous metamaterial lens show a marked improvement in the directivity and gain over using the CHDR slab. Therefore, a design of a metamaterial lens in a parabolic shape could improve the gain. In addition, after the metamaterial lens is simulated, it could then be fabricated and experimentally verified.

APPENDIX A

```matlab
%NOTE: When saving data in CST save the data as follows: the magnitude
of
%s11 as s11.txt, the magnitude of s21 as s21.txt, the phase of s11 as
%s11_arg.txt,and the phase of s21 as s21_arg.txt.
clc;
s11_mag=dlmread('s11.txt','',2,0);
format long;
s21_mag=dlmread('s21.txt','',2,0);

s11_arg=-1.*dlmread('s11_arg.txt','',2,0);
s21_arg=-1.*dlmread('s21_arg.txt','',2,0);

%convert magnitude and phase of s11 and s21 into a complex number
s11= s11_mag(:,2).*(cosd(s11_arg(:,2))+1i*sind(s11_arg(:,2)));
s21= s21_mag(:,2).*(cosd(s21_arg(:,2))+1i*sind(s21_arg(:,2)));



%impedance has a both positive and negative answer
z_pos = (((1+s11).^2-s21.^2)./((1-s11).^2-s21.^2)).^.5);
z_neg = -1.*z_pos;
% used to determine the values for the imaginary part of the refractive
% index.

z=zeros(length(z_pos),1);
for i=1:length(z_pos)

        if real(z_pos(i))>=0
            z(i)=z_pos(i);
        else
            z(i)=z_neg(i);
        end
end
z_real=real(z);
e_inkd_pos=(s21./(1-s11.*((z_pos-1)./(z_pos+1))));
e_inkd_neg=(s21./(1-s11.*((z_neg-1)./(z_neg+1))));
e_inkd=zeros(length(e_inkd_pos),1);
d=0.0025;
f=(10^9).*s11_mag(:,1);
vp=3E8;
lamda=vp./f;
k=(2*pi)./lamda;
n_pos=(imag(log(e_inkd_pos))-1i.*real(log(e_inkd_pos)))./(k.*d);
n_neg=(imag(log(e_inkd_neg))-1i.*real(log(e_inkd_neg)))./(k.*d);
n=zeros(length(n_pos),1);

for i=1:length(n)

        if imag(n_pos(i))>=0
            n(i)=n_pos(i);
```

```matlab
            z(i)=z_pos(i);
            e_inkd(i)=e_inkd_pos(i);
        else
            n(i)=n_neg(i);
            z(i)=z_neg(i);
            e_inkd(i)=e_inkd_neg(i);
        end
end
z_imag=imag(z);
epsilon=n./z;
mue=n.*z;

% the plot of the imaginary part of the refractive index.


figure(1)
hold on
plot(f,s11_mag(:,2),'g');
plot(f,s21_mag(:,2),'r');
axis([0 20E9 0 1]);
legend('s11','s21');
title('s-parameters vs frequency');
xlabel('frequency');
ylabel('Magnitude of S');
hold off

figure(2)
hold on
plot(f,(pi/180).*s11_arg(:,2),'g');
plot(f,(pi/180).*s21_arg(:,2),'r');
axis([0 20E9 -5 2]);
legend('s11','s21');
title('Phase of S vs frequency');
xlabel('frequency');
ylabel('Phase of S(radians)');
hold off

figure(3)
hold on
plot(f,real(n),'g');
plot(f,imag(n),'r');
axis([0 20E9 -6 10]);
legend('Re(n)','Im(n)');
title('refractive index vs frequency');
xlabel('frequency');
ylabel('refractive index');
hold off

figure(4)
hold on
axis([0 20E9 -2 2]);
plot(f,z_real,'g');
plot(f,z_imag,'r');

legend('Re(z)','Im(z)');
```

```matlab
title('impedance vs frequency');
xlabel('frequency');
ylabel('impedance(z)');
hold off

figure(5)
hold on
axis([0 20E9 -20 3]);
plot(f,real(epsilon),'g');
plot(f,imag(epsilon),'r');

legend('Re(epsilon)','Im(epsilon)');
title('permittivity vs frequency');
xlabel('frequency');
ylabel('permittivity');
hold off

figure(6)
hold on
axis([0 20E9 -10 15]);
plot(f,real(mue),'g');
plot(f,imag(mue),'r');

legend('Re(mue)','Im(mue)');
title('permeability vs frequency');
xlabel('frequency');
ylabel('permeability');
hold off
```

References

[1]   V. G. Veselago, "The Electrodynamics of substances with simultaneous negative values of ϵ and µ " *Soviet Physics Uspekhi,* vol. 10, p. 6, 1968.

[2]   D. R. Smith*, et al.*, "Electromagnetic parameter retrieval from inhomogeneous metamaterials," *Physical Review E - Statistical, Nonlinear, and Soft Matter Physics,* vol. 71, pp. 036617/1-036617/11, 2005.

[3]   X. Chen*, et al.*, "Robust method to retrieve the constitutive effective parameters of metamaterials," *Physical Review E - Statistical, Nonlinear, and Soft Matter Physics,* vol. 70, pp. 016608-1-016608-7, 2004.

[4]   J. B. Pendry, "Negative refraction," *Contemporary Physics,* vol. 45, p. 13, 2004.

[5]   J. B. Pendry, "Negative refraction makes a perfect lens," *Physical Review Letters,* vol. 85, pp. 3966-3969, 2000.

[6]   "Microwave Studio Simulation Software," ed, 2010.

[7]   S. A. Ramakrishna and J. B. Pendry, "Removal of absorption and increase in resolution in a near-field lens via optical gain," *Physical Review B - Condensed Matter and Materials Physics,* vol. 67, pp. 2011011-2011014, 2003.

[8]   W. H. Weedon and C. M. Rappaport, "A general method for FDTD modeling of wave propagation in arbitrary frequency-dispersive media," *IEEE Transactions on Antennas and Propagation,* vol. 45, pp. 401-410, 1997.

[9]   B. Camps-Raga and N. E. Islam, "Optimized simulation algorithms for fractal generation and analysis," *Progress In Electromagnetics Research M,* vol. 11, pp. 225-240, 2010.

[10]   L. Solymar and E. Shamonina, *Waves in metamaterials*. Oxford ; New York: Oxford University Press, 2009.

[11]   M. N. O. Sadiku, *Elements of electromagnetics*, 4th ed. New York: Oxford University Press, 2007.

[12]   J. Kim and A. Gopinath, "Simulation of a metamaterial containing cubic high dielectric resonators," *Physical Review B - Condensed Matter and Materials Physics,* vol. 76, 2007.

[13]   F. T. Ulaby, *Fundamentals of applied electromagnetics*, 5th ed. Upper Saddle River, NJ: Pearson/Prentice Hall, 2007.

[14]   P. G. Huray, *Maxwell's equations*. Hoboken, N.J.: Wiley : IEEE Press, 2010.

[15]   N. Fang*, et al.*, "Sub-diffraction-limited optical imaging with a silver superlens," *Science,* vol. 308, pp. 534-537, 2005.

[16]   F. d. Fornel, *Evanescent waves : from Newtonian optics to atomic optics*. Berlin ; New York: Springer, 2001.

[17]   T. J. Cui*, et al.* (2010). *Metamaterials theory, design, and applications*.

[18]   C. A. Balanis, *Advanced engineering electromagnetics*. New York: Wiley, 1989.

[19]   D. Courjon, *Near-field microscopy and near-field optics*. London: Imperial College Press, 2003.

[20]   E. Hecht and A. Zajac, *Optics*, 2nd ed. Reading, Mass.: Addison-Wesley Pub. Co., 1987.

[21]   Z. B. Weng*, et al.*, "A directive patch antenna with metamaterial structure," *Microwave and Optical Technology Letters,* vol. 49, pp. 456-459, 2007.

[22]   T. Taubner*, et al.*, "Near-field microscopy through a SiC superlens," *Science,* vol. 313, p. 1595, 2006.

[23]   Q. Wu*, et al.*, "A novel flat lens horn antenna designed based on zero refraction principle of metamaterials," *Applied Physics A: Materials Science and Processing,* vol. 87, pp. 151-156, 2007.